

行政院原子能委員會 委託研究計畫研究報告

以質子束在光電晶體上進行特性改變、產生波導
(waveguide)及電極性區域反轉(domain inversion)
之材料研究

受委託機關(構): 國立虎尾科技大學
計畫主持人: 廖重賓
所內共同主持人: 楊村農
業務委託單位: 行政院原子能委員會核能研究所
計畫編號: 942001INER004

目錄

中文摘要	2
英文摘要	3
計畫目的	4
計畫緣起	5
執行方法與進度說明	6
結論與建議	20
參考文獻	23
附錄	24

中文摘要

利用質子束轟擊半導體或光電材料，可以對材料進行特性的改良或創造。這個效果是藉由質子束在材料內部產生缺陷、或改變分子排列結構的機制來達成。例子之一是半導體的後段製程設備—粒子處理站(Particle-Beam Stand)。它利用高能質子束轟擊混合信號 IC 晶片，來抑制矽基底串音[1]。我們為這個效應建立了等效的單一陷阱能階模型，利用實驗結果和電腦模擬所得的參數，推算出單一陷阱能階(E_T)在 n-Si 約為+0.24eV，在 p-Si 約為-0.34eV(均從能隙的中心起算)。

我們也提出了一個雷射駐波極化(Standing-Laser-Poling)的新方法，來對非線性鐵電材料，如鈮酸鋰，進行電極性區域反轉。這個方法可以應用在倍頻藍光晶體的製作和生產上。我們也已經對鈮酸鋰晶體，進行初步的實驗，驗證質子束對電極性區域反轉的效果。

經過數值模擬和理論推導，我們發現經由在寄主材料(host material)中，引入兩種以上不同的電偶極，可以創造出在原本電偶極之自然頻率以外的共振頻率。也就是說，經由仔細的設計，我們可以突破材料天然特性的限制，在所需要的頻率區段創造出共振吸收光譜。

Abstract

The properties of semiconductors or electro-optical materials can be improved or created by proton-beam treatment. This effect results from the mechanisms that the bombardment of proton-beam causes the defects or atomic rearrangement in the materials. One of the examples is a VLSI back-end facility, Particle-Beam Stand. This equipment uses energetic proton beams on the mixed-mode IC wafers for the suppression of substrate coupling [1]. We established an effective single-level defect dipole model for this effect and employed experimental results and numerical simulation parameters to compute the single trap level (E_T). The found E_T is at about +0.24 eV in n-Si and at -0.34 eV in p-Si, measuring from the center of the energy band-gap.

We proposed a new “standing-laser-poling” method for volumetric domain inversion of nonlinear ferroelectric media, such as LiNbO_3 . This method could be used in the preparation and fabrication of frequency-doubling blue laser crystals. We also carried out initial experiments on LiNbO_3 crystals to verify the effect of domain inversion resulted from proton-beam treatment.

After efforts of the numerical simulation and theoretical derivation, we found that the collective co-working of more than one type of implemented defect dipoles may be utilized to generate the resonance at the frequencies other than the natural frequencies of all original defect dipoles. This is to say, by way of careful designing, we can create desired resonance absorption spectrum despite limitations of natural materials.

計畫目的

現今有許多科技發展都聚焦在新光電材料、產品的開發，例如 DVD 雷射讀取頭、有機發光二極體平面顯示器等。這些產品的特性或品質，有很大部份取決於所使用材料的光電特性。利用質子束，能對這些材料的光電特性做有效的改變。質子束的應用，已經被驗證確實可以改善混合信號 IC 晶片的矽基底串音問題[2]。不過，改善的物理機制一直沒有被仔細的研究清楚。如果我們能對質子束引致的缺陷特性提出一個容易使用的模型，就能夠讓質子束的使用，有明確的理論和觀念引導，增加應用的便利性和效果。

另外，以鈦酸鋰，進行短週期(short-period)電極性區域反轉，以產生倍頻藍光的技術，能應用到下一世代的 DVD 讀取頭。我們想探討應用嶄新的方法進行區域反轉的可能性，這些方法包括有雷射駐波、質子束照射等。以期對下一世代的藍光雷射技術帶來突破。

人們在設計新材料時，常會尋求特定的電磁頻譜特性，例如在特定的頻率需要共振吸收光譜。以往常用的方法是尋找適當的天然材料或利用量子點，現在我們嘗試在材料中置入外加電偶極的新方法，來改變材料的電磁頻譜特性，如折射率的共振頻率等。Clausius-Mossotti 方程式的電腦模擬以及數學推導，是我們想要釐清的第一個關鍵。

計畫緣起

本計畫是一個兩年(94、95 年)的研究計畫，所依據的想法事實上係衍生自“以 dipole 工程改變微波、光電、光學材料及功能特性——包含：提高微波 on-chip 電感值、改變非線性光電材料特性及改造(有機)發光二極體之光譜表現等”的思惟主軸。在與核研所合作的質子束改善混合信號 IC 晶片矽基底串音情形的實驗中，偶然發現了經過質子束處理的晶片上之電感器，其電感值在某一個頻率時會有爆炸性的峰值。我們將其歸因於質子束造成的缺陷電偶極和在電感器上傳播的電磁信號之間的共振現象。這激發了我們進一步研究，在材料中植入各種不同的外加電偶極(可能是缺陷或其他極性分子)，是否能對光學性質(如共振吸收光譜)進行改良。並藉由理論分析及數值模擬，嘗試掌握共振頻率改變的規則與條件。

之前我們在進行 IC 晶片質子束實驗時，累積了許多經驗，對電偶極如何影響材料的電磁頻譜特性也有初步的掌握。只要將之前的應用轉移到光波的頻率範圍，就能對光電晶體進行特性改良，由此也可以激發出對現存問題的全新解決之道，如利用質子束進行鈮酸鋰晶體的電極性區域反轉等。因此向核研所提出本計畫，以期推進光電晶體的特性改進技術。

執行方法與進度說明

本兩年研究計畫第一年的研究工作主要聚焦於新點子的產出、初步的理論、實驗探索，工作環境／設備的安排，並發表相關文獻，以作為第二年研究工作之準備。

為了分析質子束對材料產生影響的模式，首先從對矽半導體晶片造成電阻係數上升，基板串音降低的現象開始分析。這部份已經在之前的實驗中得到充足的數據和資料，現在所要做的就是對這些資料進行分析並建立模型。我們對經過質子束處理的矽基板進行霍爾量測 (Hall measurement)，得到它的電荷載子濃度(n and p)和遷移率(μ_e and μ_h)，以及電阻率(resistivity, ρ)，數據如表一所示。所使用的質子束的能量是 30 MeV，劑量(fluence)是 $2.3 \times 10^{16} \text{ cm}^{-2}$ ，霍爾量測使用的磁場為 3000 G。

表一、霍爾量測的結果

	n-Si	p-Si
$\rho_0^{\&}$ ($\Omega\text{-cm}$)	7	7
n_0 or p_0 (cm^{-3})	5.95×10^{14}	1.98×10^{15}
μ_{e0} or μ_{h0} ($\text{cm}^2/\text{V-s}$)	1,500	500
ρ ($\Omega\text{-cm}$)	2.2×10^5	1.6×10^5
n or p (cm^{-3})	2.0×10^{11}	4.8×10^{11}
μ_e or μ_h ($\text{cm}^2/\text{V-s}$)	137	81

由這些實驗資料出發，我們首先分析要利用質子轟擊造成非晶質 (Amorphous) 矽所需的條件。結果發現，使用 10~30 MeV 的質子束，

無法在 85 K (或 -188 °C) 以上造成非晶質矽。因此我們退而求其次，利用質子束轟擊，造成半絕緣矽(semi-insulating Si)，來增加電阻率。非晶質矽的電阻率約為 10^{10} - 10^{11} Ω -cm，半絕緣矽約為 10^5 - 10^6 Ω -cm。接下來我們利用 TRIM (the Transport of Ions in Matter) 這套軟體，模擬出 30 MeV 質子束中的一個質子，在矽材料中行進時，所造成的晶格移位(缺陷，defects)平均數目約為 160 個。假設矽晶片的厚度為 5 mm，則質子束劑量(Proton fluence)，F，和總缺陷密度， N_T ，之間的關係為：

$$N_T(\text{defect/cm}^3) = \frac{F(\text{proton/cm}^2) \cdot A(\text{cm}^2) \cdot 160(\text{defect/proton})}{A(\text{cm}^2) \cdot 0.5(\text{cm})} = 320F \quad (1)$$

接下來就可以由現有的單一陷阱能階理論，配合數值擬合 (Numerically fitting)，以求得單一陷阱能階(E_T)。例如在 n-Si 的情況下(E_T 由矽的能隙中央起算)，依據準 Fermi-Dirac 統計，可得：

$$f(E_T) \equiv \frac{N_T^e}{N_T} = \frac{1}{1 + e^{(E_T - E_F)/kT}} \quad (2)$$

其中 N_T^e 是捕獲了一個電子之缺陷的密度， E_F 是缺陷建立後的準費米能量(quasi Fermi energy)，k 是波茲曼常數，T 則是絕對溫度(單位為 K)。因此，最後的平衡電子濃度(n)變成：

$$n = n_0 - N_T^e = n_0 - \frac{N_T}{1 + e^{(E_T - E_F)/kT}} \quad (3)$$

然而，因為 n 必須為正才有物理意義，上式經過整理後為：

$$E_T - E_F = kT \cdot \ln\left(\frac{N_T}{n_0} - 1\right) + \delta \quad (4)$$

δ 是一個正的能量值，而 E_F 可以用下式算出：

$$E_F = E_C + kT \cdot \ln\left(\frac{n}{N_C}\right) \quad (5)$$

其中， N_C ($= 2.8 \cdot 10^{19} \text{ cm}^{-3}$ at 300 K) 是在質子束轟擊之前，矽晶片傳導帶的有效態位密度。然後變化 δ 以符合實驗數據，可以得到 E_T 、 E_F 和 δ 如表二所示。

表二、經質子束處理過的 n-Si 晶片之單一陷阱能階參數

	Case 1	Case 2
Sample	n-Si, 7 Ω -cm	n-Si, 7 Ω -cm
n_0 (cm^{-3})	$5.95 \cdot 10^{14}$	$5.95 \cdot 10^{14}$
Proton fluence F (cm^{-2})	$7.16 \cdot 10^{15}$	$3.58 \cdot 10^{16}$
N_T (cm^{-3})	$2.29 \cdot 10^{18}$	$1.15 \cdot 10^{19}$
n (cm^{-3})	$2.75 \cdot 10^{10}$	$4.38 \cdot 10^9$
E_F (eV)	0.0415126	-0.0044588
E_T (eV)	0.2478826	0.2421732
δ (eV)	$1.2 \cdot 10^{-6}$	$2.0 \cdot 10^{-7}$

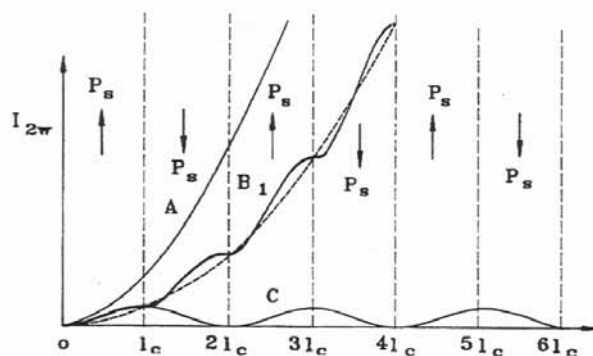
相同的方法可以應用到 p-Si 晶片的情況，所得到的 E_T 、 E_F 和 δ 如表三。

表三、經質子束處理過的 p-Si 晶片之單一陷阱能階參數

	Case 1	Case 2
Sample	p-Si, 7 Ω -cm	p-Si, 1,000 Ω -cm
p_0 (cm^{-3})	$1.98 \cdot 10^{15}$	$1.389 \cdot 10^{13}$
Proton fluence F (cm^{-2})	$2.30 \cdot 10^{16}$	$1.56 \cdot 10^{15}$
N_T (cm^{-3})	$7.36 \cdot 10^{18}$	$3.48 \cdot 10^{18}$
p (cm^{-3})	$4.72 \cdot 10^{11}$	$7.04 \cdot 10^9$
E_F (eV)	-0.1372976	-0.03216341
E_T (eV)	-0.3428148	-0.3429603
δ (eV)	$6.0 \cdot 10^{-7}$	$1.27 \cdot 10^{-5}$

在對非線性鐵電材料，如鈦酸鋰，進行電極性區域反轉的研究方面，我們也提出了一個創新的方法，就是雷射駐波極化(Standing Laser Poling)。

在鐵電性材料內部，存在有自發性的極化現象，也就是說，這些材料有內部電偶極矩。這些電偶極矩的方向可以被控制，形成我們所需要的區域配置(domain configurations)。而現在許多的科學家及研究人員將可觀的精力投入在能進行光波頻率轉換的區域配置上。尤其是可以產生二次諧波(second harmonic generation, SHG)的區域配置。這項技術可以用來產生倍頻藍光，應用在熱門的下一代高密度光儲存媒體(如藍光 DVD)。目前最受歡迎的 SHG 方法就是準相位匹配法(quasi-phase-matching, QPM) [3]。這種方法利用非線性材料內的週期性偏極化，來對入射光波和所產生的二次諧波進行相位匹配。如圖一所示。



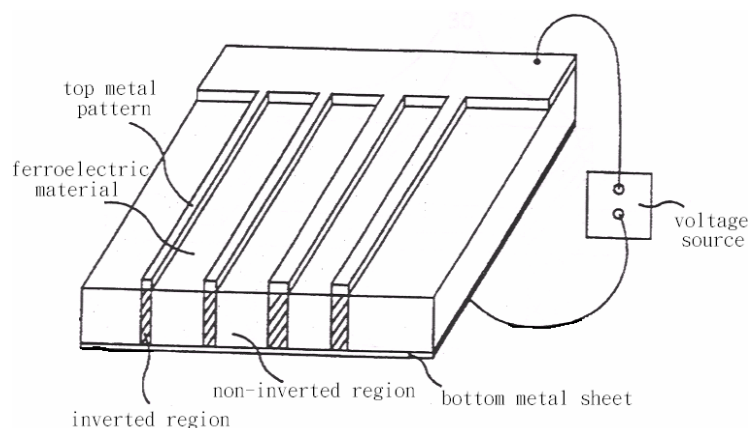
圖一、二次諧波隨晶體內行進距離增大的成長量與相位匹配的關係
上圖顯示相位匹配對二次諧波強度隨著在晶體內行進的成長量

之影響。曲線 A 表示在光波的行進路徑中，相位都完美的匹配。曲線 C 表示沒有相位匹配的情況。曲線 B_1 代表一階(first-order)QPM 的情況，它是指每經過一個同調長度(coherent length, l_c)，就把晶體內部自發偏極化(P_s)的極性反相。當 l_c 很小時，曲線 B_1 就趨近於理想情況下的曲線 A。

在藍光 DVD 讀取頭和投影電視等應用中，所需要的是短週期長度(short-pitch)的 QPM，其週期長度約為 $1.67 \mu\text{m}$ (對鋁酸鋰而言) [4],[5]。

現有造成電極性區域反轉的方法可以分成兩類，即淺(shallow)電極性區域反轉和深(volumetric)電極性區域反轉。一般而言，淺電極性區域反轉只能產生小於 $2 \mu\text{m}$ 之深度的 QPM 區域，而且其區域邊界不垂直於晶體表面，因此效率和深電極性區域反轉比起來較差。我們所提出的方法即屬為具較高效率的深電極性區域反轉。

在現在廣泛使用的深電極性區域反轉方法方面，有一種是電場極化法(Electric field poling)，如下圖所示。



圖二、電場極化法的配置圖

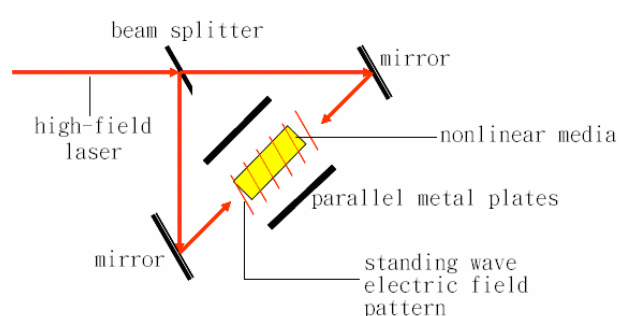
圖二中顯示了在鐵電性材料上面有一條一條狹長的金屬片，下方則是一整片金屬板。在上下兩片金屬之間加上電壓，就可以造成電極性區域反轉的區域和沒有電極性反轉的區域。這裡所採用的電場通常是脈波形式，強度需要達到 20-26 kV/mm(對鈮酸鋰而言)。因為電場在鐵電性材料裡面會有擴散的現象，因此這個方法很難得到短週期長度(l_c)的區域反轉及明確的區域邊界。對厚度為 500 μm 的鈮酸鋰晶體而言，最短的週期長度是 6 μm 。這樣的週期長度無法在鈮酸鋰晶體中產生一階(1^{st} -order)SHG 藍光。

我們所提出的方法是利用短波長(0.2~2 μm)、脈衝式高電場強度的雷射，產生駐波對非線性材料實施短週期長度的深電極性區域反轉。

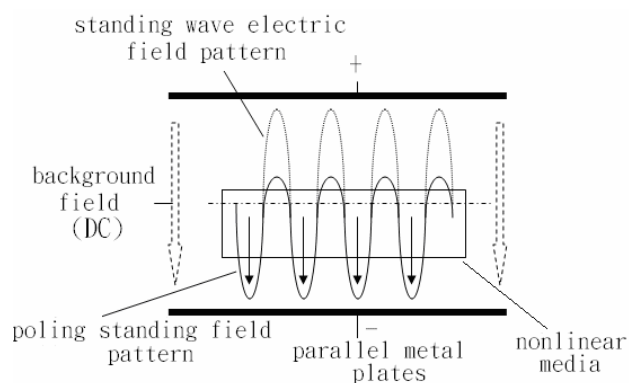
對雷射駐波而言，電場為零的節點位置不會改變，但在兩個節點間的駐波強度會隨時間呈現 $\cos(\omega t)$ 的變化(ω 就是雷射的角頻率)，也就是說，有正負極性的改變。因此，為了建立單一方向的電極性區

域反轉，需要一個額外的背景直流電場， E_{back} 。而且，假設在非線性材料中造成電極性區域反轉的臨界電場為 E_{th} ，這個方法的必要條件是：雷射駐波的電場峰值(E_0)和 E_{back} 都必須小於 E_{th} ，而(E_0+E_{back})則必須大於或等於 E_{th} 。

依據圖一，假設所需的區域週期長度是 l_c ，則高功率雷射的波長(λ)就要是($2 \cdot l_c$)。雷射駐波極化法的配置圖如圖三和圖四所示。



圖三、雷射駐波極化法的配置圖



圖四、雷射駐波電場和背景直流電場的疊加

背景直流電場是由兩個平行金屬板加上偏壓來提供。假設我們所需的 l_c 為 $0.5 \mu\text{m}$ ，雷射的波長就是 $1 \mu\text{m}$ ，利用分光片和鏡片，可以產生雷射駐波，加上背景直流電場所形成的總電場，可以提供我們所需的短週期長度區域反轉($0.5 \mu\text{m}$)。雖然總電場的大小會隨時間變化，但是每次到達峰值時，電場強度就會超過 E_{th} ，有效地進行電極

性區域反轉。

所需的雷射脈衝功率計算如下：雷射的最大功率為 $(E_0 \cdot H_0 \cdot A)$ ，磁場強度 H 等於 (B/μ_0) ， A 是雷射的光束橫截面積。假設雷射是 TEM 波， B 等於 (E_0/c) ， c 等於 $3 \cdot 10^8$ m/s，且光束直徑為 1 cm，則所需的雷射功率約為 35 MW。只有少數的脈衝雷射具有這麼高的功率以及 0.2~4 μm 的波長，舉例來說，根據[6]，一些符合需求的高功率脈衝雷射如表四所示。

表四、高功率脈衝雷射

Type	Wavelength (μm)	Pulsed power level (W)
Holmium	2.06	$>10^7$
Iodine	1.315	$>10^{12}$
Nd-glass, YAG	1.06	$\sim 10^{14}$
Ruby	0.6943	10^{10}
Kr-F	0.26	$>10^9$
Xenon	0.175	$>10^8$

為探討以質子束製造缺陷或從外植入永久電偶極 (permanent dipoles) 對光電晶體特性改變，我們這一年來終於在理論上有所突破，就是在寄主材料(host material)中植入兩種以上的電偶極，可以在原本沒有共振的頻率創造出共振吸收光譜。

在許多光學或光電的應用領域裡，常常需要讓材料或元件在特定頻率展現出折射率(或吸收光譜)的共振峰值。當沒有天然的材料可以呈現這個頻率的峰值，人們就會轉而在材料中置入人工的電偶極，如特殊的分子或化合物，使共振在該頻率出現。當這種方法也不可行

時，還可以採用在材料中置入量子點或量子井的方法。但是這種方法對複雜的處理程序、工具及原料有嚴格的要求。在這裡，我們提出的方法可以克服這些缺點。那就是利用材料中多種外加電偶極的集體作用，改變材料的光學和光電特性。

接下來將展現這個方法的數學理論推導，和數值模擬結果。我們從 Clausius-Mossotti Equation (CME) 著手。CME 描述了一個物體の色散關係，即 ω 與 k 的非線性關係，在這裡 ω 代表在物體中行進之光波的角頻率， k 則是光波的波數(wave number) [7],[8]。而這個關係決定了該物體的相對介電係數(ϵ_r)。CME 是將原子視為和光波作用的電偶極而推導出來的。我們在這裡將其用來描述寄主材料中的外加電偶極和光波的作用。

CME 的形式如下：

$$\frac{\epsilon_r - 1}{\epsilon_r + 2} = \frac{Ne^2}{3\epsilon_0 m_e} \sum_j \frac{f_j}{\Omega_j^2 - \omega^2 + i\gamma_j \omega} \quad (6)$$

其中， N 為材料中外加電偶極的總（數目）密度， ϵ_r 為外加電偶極之集總的相對介電係數， e 為電子電荷， ϵ_0 為真空介電係數， m_e 為電子靜質量， f_j 為第 j 種電偶極所佔的數目比例， Ω_j 為電偶極的自然角頻率， γ_j 代表電子的阻滯（damping）角頻率 [7],[8]。

在我們進行數值模擬實驗時，偶然發現一個現象，就是當兩種或更多的電偶極混和後，所產生的集體共振頻率，會比原來參與的電偶

極自然頻率還小(或大)。我們後來利用 CME 做數學推導，解釋了這個現象，推導過程如下：

假設第 j 種電偶極的偏極化率(polarizability)為

$e^2/(\epsilon_0 m_e \Omega_j^2) = \alpha_j$ ，並令 $\gamma_j = 2\gamma_j'$ ，以符合慣例，則 CME 變成：

$$\frac{\epsilon_r - 1}{\epsilon_r + 2} = \frac{N}{3} \sum_j \frac{\alpha_j \Omega_j^2 f_j}{(\Omega_j^2 - \omega^2 + i2\gamma_j' \omega)} \quad (7)$$

然後定義 $N_j \equiv N \cdot f_j$ ， $x_j = \omega / \Omega_j$ ， $y_j = \gamma_j' / \Omega_j$ ，(2)式就變為：

$$\frac{\epsilon_r - 1}{\epsilon_r + 2} = \sum_j \frac{\frac{1}{3} N_j \alpha_j}{1 - x_j^2 + i2x_j y_j} \quad (8)$$

在只有一種電偶極的情況下，並令 $\epsilon_r - 1 \equiv z$ ， $N_1 \alpha_1 / 3 \equiv a_1$ ，(8)

式變成 $\frac{z}{z+3} = \frac{a_1}{1 - x_1^2 + i2x_1 y_1}$ ，然後， $z \equiv \epsilon_r - 1 = \frac{3a_1}{(1 - a_1 - x_1^2) + i2x_1 y_1}$ ，因此，共振

發生在 $x_1^2 \doteq (1 - a_1)$ ，或 $\omega_{\text{res}}^2 \doteq (1 - a_1) \Omega_1^2$ 。

為了數學上的簡化，我們考慮兩種電偶極混和的情況，則 CME 變

成：

$$\frac{z}{z+3} = \frac{a_1}{1 - x_1^2 + i2x_1 y_1} + \frac{a_2}{1 - x_2^2 + i2x_2 y_2} = \frac{a_1(1 - x_2^2 + i2x_2 y_2) + a_2(1 - x_1^2 + i2x_1 y_1)}{(1 - x_1^2 + i2x_1 y_1)(1 - x_2^2 + i2x_2 y_2)} \quad (9)$$

在吾人有興趣的低阻滯情況下， $y_1 \doteq y_2 \doteq 0$ ， ϵ_r 明顯較大，(9)式

就變成：

$$(1 - x_1^2)(1 - x_2^2)z \cong [a_1(1 - x_2^2) + a_2(1 - x_1^2)]z + 3[a_1(1 - x_2^2) + a_2(1 - x_1^2)] \quad (10)$$

$$\cdot [(1 - a_1 - a_2) - (1 - a_2)x_1^2 - (1 - a_1)x_2^2 + x_1^2 x_2^2]z \approx 3[a_1(1 - x_2^2) + a_2(1 - x_1^2)] \quad (11)$$

因此，

$$[(1-a_1-a_2)\Omega_1^2\Omega_2^2 - (1-a_2)\Omega_2^2\omega^2 - (1-a_1)\Omega_1^2\omega^2 + \omega^4]z \approx 3a_1\Omega_1^2(\Omega_2^2 - \omega^2) + 3a_2\Omega_2^2(\Omega_1^2 - \omega^2) \quad (12)$$

從上式我們可以發現， z 或 ε_r 的峰值發生在(7)式的”約等於”符號左邊趨近於零的時候。令 $[(1-a_2)\Omega_2^2 + (1-a_1)\Omega_1^2] = M$ ， z 或 ε_r 的峰值頻率 (ω_{res}) 發生在：

$$\omega_{res}^2 = \frac{M \pm \sqrt{M^2 - 4(1-a_1-a_2)\Omega_1^2\Omega_2^2}}{2} = \frac{M \pm M \left(1 - \frac{4(1-a_1-a_2)\Omega_1^2\Omega_2^2}{M^2}\right)^{0.5}}{2} \quad (13)$$

在 $\Omega_2^2 \gg \Omega_1^2$ 的情況，利用二項式展開，然後捨去高次項，可得：

$$\omega_{res}^2 = \frac{M \pm M \left(1 - \frac{2(1-a_1-a_2)\Omega_1^2\Omega_2^2}{M^2}\right)}{2} \quad (14)$$

因此 ω_{res}^2 會近似於下列兩個值：

$$(a) \quad \omega_{res}^2 \cong (1-a_2)\Omega_2^2 + (1-a_1)\Omega_1^2$$

$$(b) \quad \omega_{res}^2 \cong \frac{(1-a_1-a_2)\Omega_1^2\Omega_2^2}{(1-a_2)\Omega_2^2 + (1-a_1)\Omega_1^2}$$

由情況(a)，我們得到 $\omega_{res} > \max(\Omega_1, \Omega_2)$ (當 a_1 和 a_2 均很小時)。

另一方面，由情況(b)，當 $\Omega_2^2 \gg \Omega_1^2$ ，我們得到：

$$\omega_{res}^2 \cong \frac{1-a_1-a_2}{1-a_2}\Omega_1^2 \quad (15)$$

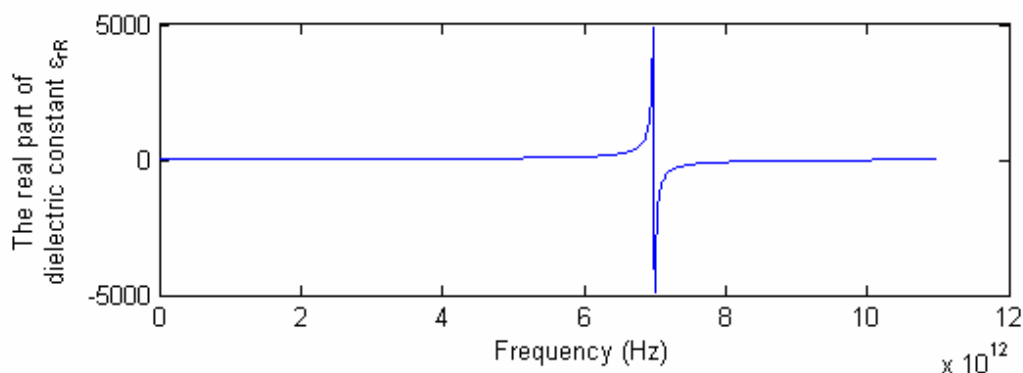
如果上式中的 ω_{res} 小於只用一種電偶極的情況(即

$\omega_{res}^2 \doteq (1-a_1)\Omega_1^2$)，「集體共振頻率向前推移」的現象就產生了。

我們發現，因為 $1-a_2 > 0$ ，而且 $(1-a_1-a_2) < (1-a_1)(1-a_2)$ ，「共振頻率向前推移」在理論上被證實了。而其原因(主要是 $y_1 \doteq y_2 \doteq 0$ 、

$a_1 \ll 1$ 、 $a_2 \ll 1$ 、和 $\Omega_2^2 \gg \Omega_1^2$) 也已經瞭解。

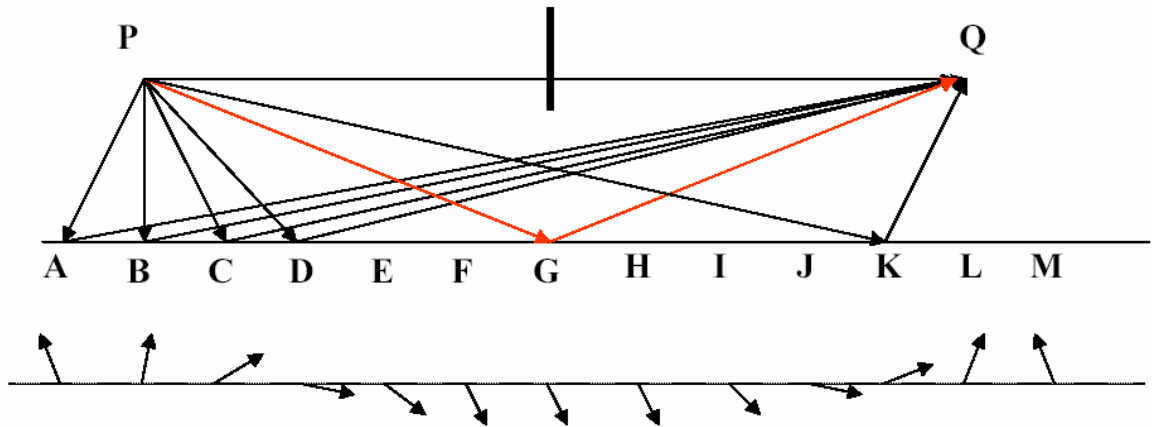
圖五顯示了在寄主材料中植入兩種電偶極的情況。其中 $N_1 = 1 \times 10^{23} \text{ m}^{-3}$ ， $\Omega_1/2\pi = 1 \times 10^{13} \text{ Hz}$ (而且 $y_1 = 5 \times 10^{-4}$ ， $a_1 = 0.0269$) 以及 $N_2 = 3 \times 10^{25} \text{ m}^{-3}$ ， $\Omega_2/2\pi = 3 \times 10^{13} \text{ Hz}$ (而且 $y_2 = 5 \times 10^{-4}$ ， $a_2 = 0.8960$)。所產生的集體共振頻率在 $6.9 \times 10^{12} \text{ Hz}$ ，小於參與混和的兩種電偶極之自然共振頻率。



圖五、在兩種電偶極混和情況下，共振頻率向前推移現象顯著發生的例子

以上的理論及數值模擬結果，目前正在準備發表中。相關質子束轟擊 ITO 實驗也為了配合此新的發現而正在調整較佳參數。

共振頻率向前推移，就好像在我們需要的頻率，多了原本不存在的”幽靈”電偶極產生的介電係數峰值。因為物體的折射率 ($n = \epsilon_r^{1/2}$)，所以這個方法可以產生各式各樣作用在廣大頻率範圍的電磁波反射元件。其中，一種”奇妙的”鏡子，具有入射角不等於反射角之特性，就可以透過這種方法製作出來，如圖六。



圖六、利用多種電偶極所產生的集體折射率增強效果製作” 奇妙的” 鏡子
 假設在利用前述” 幽靈” 電偶極現象製作的反射鏡上面的 P
 點，有一個光源。根據量子力學的觀點，這個光源的光可以沿著無限
 多條路徑到達同樣在反射鏡上面的 Q 點。現在將鏡子右邊 $\frac{3}{4}$ 的部分去
 掉，只剩下圖中 A、B、C 點附近的部份。依據傳統光學，光線不可能
 由 P 點經由反射到達 Q 點，但是根據量子力學，則可以令光線由 P 點
 出發，經過 A 點，到達 Q 點(即 L_{PAQ} 路徑)。只要找出所有由 P 點經過
 反射到達 Q 點的路徑中，和 L_{PAQ} 長度相差不是整數倍波長的，將這些
 路徑經過的鏡子部分去掉。就可以令剩下到達 Q 點的光線，都具有相
 同的相位。如此一來，建設性干涉就會使光線聚集足夠的強度，由 P
 點出發，經過 A 點，到達 Q 點。

以上的成果，已寫成三篇技術文獻(如附錄)，如下所示：

1. Chungpin Liao, T. S. Duh, T. N. Yang, S. M. Lan, C. W. Liu,
 T. T. Yang, J. S. Hsu, H. Y. Shao, “An Effective
 One-Trap-Level CAD Model for the General SOC Integration

Platform -- Particle-Beam Stand (PBS) -- When Modeling Proton-Caused Local Semi-Insulating Regions” , P12, 2004 Semiconductor Manufacturing Technology Workshop (SMTW), Hsinchu, Taiwan, 9-10 Sep. 2004.

2. “Standing-laser-poling for Implementing Short-Pitch Periodic Domain Inversion In Ferroelectric Media” (Submitted to IEEE Selected Topics in Quantum Electronics, 2005).
3. “Creation of Resonance Frequencies and Enhancement of K by Collective Defect Interactions and Their Novel Applications” (To be further modified and submitted to an international journal).

第一篇已發表於 SMTW 國際研討會，第二篇方投稿 IEEE Selected Topics in Quantum Electronics，第三篇初稿已完成，正待進一步補強內容以投稿國際期刊。

我們也進行了質子束對鋯酸鋰電極性區域反轉效果的初步實驗和評估。儘管以 200-400 keV 之質子作轟擊實驗，事後蝕刻結果發現是產生局部晶體缺陷而並非所欲的集體晶格移動，但這項寶貴的資料將有助於導引下一階段的實驗(如：罩幕 (masking) 及劑量的改變)。

結論與建議

在質子束對材料內部結構和電阻特性所產生的影響評估方面，我們建立了一個容易使用的數學模型，大幅加速以後應用質子束時的分析工作。我們是依據單一陷阱能階模型來計算，並建議質子轟擊所產生的缺陷應具有非零的電荷量，可以散射在材料內部行進的電子。除了散射以外，缺陷還會捕獲電子，這一點可以經由量測結果中的載子數大幅減少證明。依據我們的計算結果，單一陷阱能階(E_T)距離價帶頂部和導帶底部都有一段距離(在 n-Si 中， E_T 為 +0.24 eV，在 p-Si 中為 -0.34 eV，均從能隙中心量起)，所以可以得知，質子束所造成的缺陷具有電子活性(可以捕獲電子或放出電子)，造成矽晶體電阻率上升、串音雜訊減少。

我們所提出的雷射駐波極化法，可以對非線性鐵電材料，進行短週期長度(short pitch)的電極性區域反轉。例如利用高功率的脈衝雷射，對鈮酸鋰進行 0.2~2 μm 週期長度的準相位匹配(QPM)。這個方法可以利用雷射所具有的短波長，在鈮酸鋰晶體上進行倍頻藍光的一階(1st-order)QPM。根據我們的估計，現有的高功率脈衝雷射(~10 MW)可以派上用場，因為所需要的雷射頻率約為 10^{14} Hz，因此電極性區域反轉可以由持續 10 ms 的雷射脈衝週期中之極多次重複極化動作來完成。

這個方法的細節還需要經過實驗來印證，但是此法在另一個重要領域也有很大的發展空間，就是光子晶體(Photonic crystal)的製造。就像特殊結構的矽晶體(如二極體)可以控制電流的流通，在空間區域的配置上有特殊結構的光子晶體也可以控制光線的傳導。例如在PPLN(periodically poled lithium niobate)晶體內部，安排鐵電性區域的大小、分佈及週期性，可以形成一個”設計(designer)”材料，應用於光線的處理上。這個新興的研究領域，也值得我們更進一步的投入。

在各種光學和光電的應用中，常會需要在特定的頻率範圍，設計一個折射率(或吸收光譜)的共振峰值，或改變折射率頻譜的特性與形狀。但是，天然材料的共振頻譜是固定的，其共振頻率也不一定符合我們的需要。因此，有時候人們會以植入量子點或量子井的方式來產生人工的光譜特性。但這種方式需要繁複及高精密度的手續，成本高昂。

我們在利用 Clausius-Mossotti Equation (CME)，模擬質子束所造成的缺陷偶極對光譜特性的影響時，偶然發現了一個現象，就是當寄主材料中有兩種以上的外加電偶極時，會在原本電偶極的自然共振頻率之外，產生一個介電係數的集體共振峰值。就好像出現了一個原本不存在的”幽靈”電偶極，造成新的共振頻率。我們稱這種現象

為集體共振頻率的向前(向後)推移。經過良好的設計，在寄主材料中植入多種外加電偶極，可以在我們想要的特定頻率創造出折射率峰值，這個新的方法克服了現有途徑所遇到的困難，提供了設計材料電磁共振頻率的另一種選擇。我們從 CME 著手，推導出了集體共振頻率推移現象的成因和條件，也執行了數值模擬，觀察這種現象的詳細特性。

我們還延伸出了一個新點子，就是利用多種外加電偶極的集體共振現象，製作一種奇妙的鏡子，可以呈現入射角不等於反射角的特性。它是利用多種外加電偶極的集體共振，提供材料在寬頻率範圍內的反射效果。加上量子力學中，光子會沿所有可能路徑前進的觀點，刪除破壞性干涉的鏡面，只留下建設性干涉，來製作這種特殊的”鏡子”。

綜合以上，本年度研究計畫之執行堪稱頗見一些當初預估但並沒有把握的好結果而且頗具前瞻應用性，值得第二年再加倍努力。

參考文獻

1. C. P. Liao, D. Tang, H. C. Lu, "Creation of local semi-insulating regions on semiconductor substrates," US Patent 6,046,109, April 4, 2000.
2. C. P. Liao, M. N. Liu, and K. C. Juang, "Cross-talk suppression in mixed-mode IC's by the π technology and the future with a SOC integration platform: particle-beam stand (PBS)," IEEE Transactions on Electron Devices, vol. 50, pp 764-768, Special Issue on RF and SOC, March 2003.
3. Fejer, M. M., "Quasi-Phase-Matched Second Harmonic Generation: Tuning and Tolerances," *IEEE Journal of Quantum Electronics*, Vol. 28, No. 11, 1992.
4. Nelson, D. F. and Mikulyak, *J. Appl. Phys* **45**, 3688 (1974).
5. Jundt, D. H., *Optics Letters*, **22**, 1553 (1997).
6. US Naval Research Laboratory, *Plasma Formulary*, p. 50, 1987.
7. G. Bekefi and A. H. Barrett, *Electromagnetic Vibrations, Waves, And Radiation*, pp. 435-437, MIT Press, Cambridge (1977).
8. M. A. Omar, *Elementary Solid State Physics*, pp. 376-384, Addison-Wesley, Reading Massachusetts (1993).

附錄

Published in SMTW (Semiconductor Manufacturing Technology Workshop) 2004

An Effective One-Trap-Level CAD Model for the General SOC Integration Platform -- Particle-Beam Stand (PBS) -- When Modeling Proton-Caused Local Semi-Insulating Regions

Chungpin Liao^{1,2}, T. S. Duh³, T. N. Yang³, S. M. Lan³, C. W. Liu⁴, T. T. Yang³, J. S. Hsu¹, H. Y. Shao²

¹ Graduate Institute of Electro-Optical and Material Science
National Huwei University of Science and Technology (NHUST)

² Advanced Research & Business Laboratory (ARBL)

³ Institute of Nuclear Energy Research (INER)

⁴ Department of Electronics Engineering, National Chiao-Tung University
Huwei, Yunlin, Taiwan ROC

cpliao@alum.mit.edu

Abstract – A π technology (= particle-enhanced isolation) was proposed to employ energetic proton beams on the already-manufactured mixed-mode IC wafers (prior to packaging) for the suppression of undesirable substrate coupling [1]. However, up to this day the physics behind this proton-caused defect phase is never clear. An effective 1-level defect model is constructed using experimental results and existing single-trap-level theory [2] and TRIM (or SRIM) [3] code-simulated parameters. The found effective single trap level (E_T) is at about +0.24 eV in n-Si and at -0.34 eV in p-Si, measuring from the center of the energy band-gap.

INTRODUCTION

The π technology (= PEI = particle-enhanced isolation) was proposed to employ energetic proton beams on the already-manufactured mixed-mode IC wafers (prior to packaging) at pre-determined locations for the suppression of undesirable substrate coupling [1]. Subsequent experimental results confirmed that an improvement of 25-30 dB was easily achieved by applying a relatively low-fluence proton bombardment on the isolation-intended region within a metal pads pattern [4]. Other experiments demonstrated that great enhancement of 100-300 % on Q values of on-chip spiral inductors was readily achieved [5][6]. It was thus speculated that this technology may find its convenient use in the broad spectrum of various emerging SOC devices and may even bring substantial impact to the economical and strategic aspects of the future microelectronics production in general.

To this point, the verified success of proton-beam treatment in both the device isolation and the passives' Q-improvement on Si substrates has now enticed some big chipmakers, such as the TSMC (Taiwan Semiconductor Manufacturing Company), into realizing a pilot VLSI back-end facility: the particle-beam stand (PBS). The PBS, particularly when with its design-rules carried over to the VLSI front-end, can potentially end the traditionally laborious mixed-mode product development cycle and eventually become the general SOC integration platform. It is nonetheless a deficiency that such an approach lacks the quantitative theoretical basis, particularly a simple, effective model, to facilitate the carrying-over of PBS design rules to the VLSI front-end TCAD (technology computer-aided design) simulation environments for SOC ASICs (application-specific ICs) to emerge. This work is thus aimed to help achieve that goal by presenting an effective single-trap-level model of experimentally justified parameters.

In the following, an exploration of the ultimate degree of resistivity enhancement accessible by protons on silicon wafers is conducted first. Existing models and formulas are put under examination and their validity determined. Readers will find that making deep or through-wafer amorphous Si regions is rather impractical, in addition to the fact that it is not even feasible under the room temperature condition. Instead, the semi-insulating state is sufficient for most goals in microelectronics applications. Then, the construction of an effective one-defect-level model for such phase is attempted. This is accomplished by comparing existing one-level formulary with the outcomes of TRIM code [3] Monte-Carlo simulations, proton bombardment experiments [5] and Hall measurements [4]. Finally, a summary and conclusions are given.

THE DESIRED HIGH RESISTIVITY Si:
AMORPHOUS OR SIMPLY SEMI-INSULATING?

When energetic ions strike a silicon substrate, they lose energy in a series of nuclear and electronic collisions (called nuclear stopping and electronic stopping, respectively), and rapidly come to rest at their projection ranges. Only the nuclear collisions result in the desired displaced silicon atoms and thus crystal defects. Derivations and estimations of the minimum required ion irradiation fluence to convert the crystalline silicon into an amorphous layer have been conducted by many sources from a number of different viewpoints [7]. However, most of them overlooked the fact that *not* all ion energy are dissipated on the bond-breakings among Si lattice and thus are not correct descriptions. Only the phenomenological model by Morehead and Crowder [8] gives the fact a credible account. It also offers better description of the atomic level behavior -- dynamic annealing -- during the ion bombardment. In modeling the later, those displaced atoms are seen to reform bonds and change their position to settle on a relatively stable phase in a time period of the order of several 10^{-9} s. During this period, vacancies escape via thermal diffusion from the disordered (amorphous) core (cylinder of radius R_0) surrounding the ion track (see Fig. 1). The escaped outer sheath, of width δR (actually temperature-dependent), becomes crystalline again. Thus, the ultimate stable radius of the amorphous region is $R_0 - \delta R$. It is then clear that the number density of these amorphous cylinders (or ion fluence $D(T)$) required to overlap and form a continuous amorphous layer, i.e., $(R_0 - \delta R)^{-2}$, depends on the original average size of damage, R_0 , and the temperature-dependent out-diffusion of vacancies which reduce the damage cylinder size an amount δR .

That is,

$$D_0 \equiv D(0K) = R_0^{-2}$$

(1)

$$D(T) = (R_0 - \delta R)^{-2} = D_0 (1 - \delta R / R_0)^{-2}$$

(2)

In order to determine D_0 (or R_0), the following relation is employed,

$$\bar{E} \cdot (dE / dx)_0^{-1} \cdot (\pi R_0^{-2}) \cdot n_2 = D_0 \cdot (\pi R_0^2) \quad , \quad \text{or}$$

(3)

$$D_0 = \bar{E} n_2 (dE / dx)_0^{-1} \text{ cm}^{-2}$$

(4)

where \bar{E} is the effective energy to displace a target lattice atom in eV (~ 15 eV for Si [3]), n_2 is the target atomic number density in cm^{-3} ($= 5 \times 10^{22} \text{ cm}^{-3}$ for Si), and $(dE / dx)_0$ is the energy-independent nuclear stopping power (energy loss per unit path length).

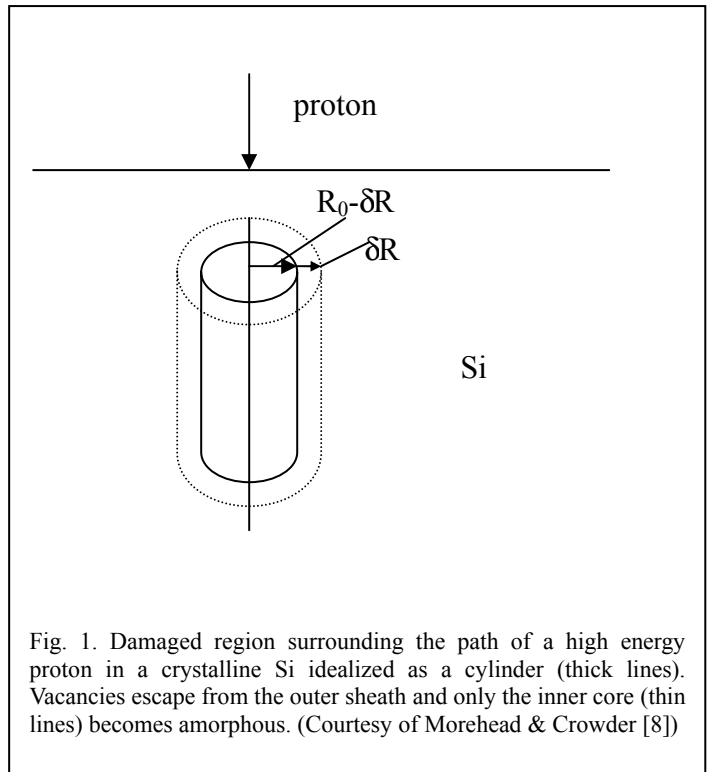


Fig. 1. Damaged region surrounding the path of a high energy proton in a crystalline Si idealized as a cylinder (thick lines). Vacancies escape from the outer sheath and only the inner core (thin lines) becomes amorphous. (Courtesy of Morehead & Crowder [8])

Note that in estimating the nuclear stopping power, Nielson's formula fails to give correct results for the proton bombardment case (use in [8]). Instead, the authors suggest that TRIM (or SRIM [3]) code simulation should be conducted for each specific case and that $(dE / dx)_0$ be obtained by averaging over the whole proton slowing down scenario. For example, for protons of energy ranging from 10 to 30 MeV of practical interest, the nuclear stopping power $(dE / dx)_0 \approx 10^{-3} \text{ keV}/\mu\text{m}$ ($= 10^4 \text{ eV}/\text{cm}$) is obtained from TRIM simulation, as compared to the unrealistically large $\sim 5 \text{ keV}/\mu\text{m}$ ($= 5 \times 10^7 \text{ eV}/\text{cm}$) from using Nielson's formula.

With this in mind, the original result of Morehead and Crowder [8] can then still be used, which is derived from equation (3), after linking δR with the diffusion process, i.e.:

$$D(T) = D_0 \cdot [1 - k'(dE / dx)_0^{-1/2} e^{-U / KT}]^{-2} \quad (5)$$

where, after fitting available experimental data from bombardment of Si by B, P, As, Sb, Bi, K' was found to be $115 (\text{keV}/\mu\text{m})^{1/2} (= 3.6 \times 10^5 (\text{eV}/\text{cm})^{1/2})$ and U was 0.06 eV [8]. Thus, from equation (3), $D_0 \approx 10^{19} \text{ cm}^{-2}$ for 30 MeV proton bombardment on Si is obtained. Further, it is noted that, from equation (5), the maximum temperature at which D (T) still exists (i.e., non-negative or physical) is when:

$$1 > K'(dE/dx)_0^{-1/2} e^{-U/KT} \quad (6)$$

In other words, for 10-30 MeV protons, the amorphous Si state cannot be reached above 85 K (or -188 °C) of the target temperature.

Realistic irradiation fluences of interest range from 10^{15} to 10^{17} ions/cm² (i.e., 0.1-10 $\mu\text{A-h}$) for MeV protons of beam size of several centimeters in diameter. This is far below $D_0 (\approx 10^{19} \text{ cm}^{-2})$ required to render the amorphous Si state under very low temperature condition. Therefore, for practical purposes, the alternative of rendering so-called “semi-insulating” Si should be pursued instead. Resistivities of amorphous and semi-insulating silicon are approximately 10^{10} - $10^{11} \Omega\text{-cm}$ and 10^5 - $10^6 \Omega\text{-cm}$, respectively.

DETERMINATION OF EFFECTIVE TOTAL DEFECT DENSITY N_T BY TRIM SIMULATION

Using 1,000 to 10,000 protons to secure meaningful statistics of a TRIM simulation, the relation between the proton fluence F and total defect density N_T , of an average 30 MeV proton bombarding on a 5 mm thick Si wafer, for example, can be obtained as follows. From TRIM, it was found that each average proton created 160 dislocations (defects) in its path through the Si wafer. Hence,

$$\begin{aligned} N_T (\text{defect} / \text{cm}^3) &= \frac{F(\text{proton} / \text{cm}^2) \cdot A(\text{cm}^2) \cdot 160(\text{defect} / \text{proton})}{A(\text{cm}^2) \cdot 0.5(\text{cm})} \\ &= 320F \end{aligned} \quad (7)$$

Similarly, each average 6 MeV proton creates approximately 65 defects along its path within its projection range in Si (i.e., $\sim 291 \mu\text{m}$) and hence $N_T = 2,229F$ (defects/cm³) within a Si substrate of thickness of about 291 μm .

CONSTRUCTION OF THE EFFECTIVE ONE-TRAP-LEVEL MODEL

Intrinsic charge state of all N_T defect

It can be seen from Hall measurement results (i.e., Table 1) that great reduction in both the charge carrier number densities (n and p) and mobilities (μ_e and μ_h) was caused by proton irradiation. The observed increase in resistivity was thus a manifestation of both effects combined. In order for the mobilities to decrease, some form of scattering must have been at work. In our case, the main mechanism is suspected to be the free carrier scattering off the charged impurities (including charged defects). Namely, the proton-created defects may each be treated as intrinsically charged when born (even without trapping any free carrier), possibly due to local charge imbalance (or, strain field) rendered by the atomic lattice distortions. Furthermore, it is suspected (as will be verified in the following) that in order to cause severe free carrier removal as observed, they should also be very effective in trapping free charges. Namely, they ought to occupy a somewhat deep trap level or bands in the energy gap between the conduction and valence edges. In other words, they can trap and release free carriers inasmuch as they each possesses fixed intrinsic charge already. In the next, we will start to secure an effective and self-consistent one-level model for both physics understanding and SOC integration applications.

Single-trap-level system

Single-level trap theory has been well developed [2] and is ready for further manipulation to extract physics and parameters of interest. In this picture, a trap can either trap an electron or not trap an electron, and thus N_T is divided into N_T^e and N_T^{ne} , respectively. If the traps are of acceptor type, then at thermal equilibrium the total defect number density N_T can be divided into N_T^{ne} (no trapping of electron, $\equiv N_T^0$) and N_T^e (with one electron trapped, $\equiv N_T^-$). Here the superscripts “0” and “-” simply mean “trapping a free electron or not” and *do not* reveal information about the net charge state on each trap. Similarly, for donor type traps, $N_T^e = N_T^0$, and $N_T^{ne} = N_T^+$ (again, $N_T = N_T^e + N_T^{ne}$). It will be shown later that for proton bombardment of interest, these created traps are of acceptor type in n-Si, and of donor type in p-Si. In the following formula manipulations and calculations, the case of proton treatment on n-Si is assumed. Then, results associated with p-Si will also be revealed.

n-Si.

At electron thermal equilibrium, the charge trapping distribution among aforementioned defects should follow the quasi Fermi-Dirac distribution $f(E_T)$, where E_T (all energy levels being measured from 0 eV at the middle of the Si energy band-gap) is the sought-for effective single trap energy level. That is, for the non-degenerate case,

$$f(E_T) \equiv \frac{N_T^e}{N_T} = \frac{1}{1 + e^{(E_T - E_F)/kT}} \quad (8)$$

where E_F is the newly adjusted quasi Fermi energy after the creation of defects, while k and T are Boltzmann constant and temperature in Kelvin, respectively. Therefore, the final equilibrium electron concentration becomes:

$$n = n_0 - N_T^e = n_0 - \frac{N_T}{1 + e^{(E_T - E_F)/kT}} \quad (9)$$

However, since this final electron concentration has to be positive to be physically meaningful, a little manipulation of equation (9) gives:

$$E_T - E_F = kT \cdot \ln \left(\frac{N_T}{n_0} - 1 \right) + \delta \quad (10)$$

where δ is a positive energy quantity, and E_F is evaluated by:

$$E_F = E_C + kT \cdot \ln \left(\frac{n}{N_C} \right) \quad (11)$$

where $N_C (= 2.8 \cdot 10^{19} \text{ cm}^{-3}$ at 300 K) is the effective density of states in the conduction band of a silicon crystal prior to proton treatment. We now obtain the associated E_T , E_F , and δ values for each case in Table 2.

p-Si.

Similarly, for p-Si cases, the hole trapping distribution among proton-created defects obeys the commentary quasi Fermi-Dirac distribution, i.e., $1 - f(E_T)$, where E_T is the trap level within p-Si. It is,

$$\frac{N_T^+}{N_T} = 1 - f(E_T) = \frac{1}{1 + e^{(E_F - E_T)/kT}} \quad (12)$$

Since the final hole concentration p has to be positive physically, we have:

$$p = p_0 - N_T^+ > 0, \text{ or } e^{(E_F - E_T)/kT} > \frac{N_T}{p_0} - 1 \quad (13)$$

where $E_F = E_V + kT \cdot \ln \left(\frac{N_V}{p} \right)$, with $N_V (= 1.04 \cdot 10^{19} \text{ cm}^{-3}$ at 300 K) the effective density of states in the valence band of a silicon crystal prior to proton treatment. Again, it is only when $N_T/p_0 > 1$ that equation (13) offers quantitatively useful information about the effective energy level E_T . In fact, $N_T/p_0 \gg 1$ is always the domain of practical interest. Hence,

$$E_F - E_T = kT \cdot \ln \left(\frac{N_T}{p_0} - 1 \right) + \delta \quad (14)$$

By varying δ to fit experimental data, parameters of the effective single-level model can be found (see Table 3).

SUMMARY & CONCLUSIONS

It was found that amorphous Si cannot be practically achieved and thus semi-insulating Si should be pursued for implementing the general SOC integration platform -- PBS. It was further suggested that these proton-created defects were intrinsically charged and all contributed to the Rutherford-like scattering of free charge carriers, and thus leading to great reduction of carrier mobilities. Note that this is true even if they do not trap any free charge, though we know they actually do as evidenced from the observed great carrier removal. In reality, in this effective single-level picture, they are also slightly active electronically (namely they would donate or accept free charges) as is obvious from the revealed somewhat deep locations of the effective single trap level in the band-gap. That is, under the low-current proton beam treatment, and in the $N_T \gg n_0$ or p_0 domain of practical interest, the effective single trap level E_T was found to be about +0.24 eV in n-Si and -0.34 eV in p-Si, as measured from the center of the energy band-gap of the Si single crystal.

REFERENCES

- [1] C. P. Liao, D. Tang, H. C. Lu, "Creation of local semi-insulating regions on semiconductor substrates," US Patent 6,046,109, April 4, 2000.

- [2] Moll J. L. Physics of Semiconductors. New York: McGraw-Hill, 1964, ch 6.
- [3] SRIM -- The Stopping and Range of Ions in Matter, a computer code constantly updated by Ziegler J. F. and Biersack J. P., and available at Internet website: <http://www.srim.org/>.
- [4] C. P. Liao, M. N. Liu, and K. C. Juang, "Cross-talk suppression in mixed-mode IC's by the π technology and the future with a SOC integration platform: particle-beam stand (PBS)," IEEE Transactions on Electron Devices, vol. 50, pp 764-768, Special Issue on RF and SOC, March 2003.
- [5] C. P. Liao, T. H. Huang, C. Y. Lee, D. Tang, S. M. Lan, T. N. Yang, L. F. Lin, "Method of creating local semi-insulating regions on silicon wafers for device isolation and realization of high Q inductors," IEEE Electron. Dev. Lett., vol. 19, pp 461-462, December 1998.
- [6] C. P. Liao, C. W. Liu, and Y. M. Hsu, "Observation of explosive spectral behaviors in proton-enhanced high-Q inductors and their explanations," IEEE Transactions on Electron Devices, vol. 50, pp 758-763, Special Issue on RF and SOC, March 2003.
- [7] S. Wolf and R. N. Tauber, Silicon Processing for the VLSI Era, vol. 1, Lattice Press, Sunset Beach, California, 1986.
- [8] F. F. Morehead Jr. and B. L. Crowder, "A model for the formation of amorphous Si by ion bombardment," Radiation Effects, vol 6, pp 27-32, 1970.

	n-Si	p-Si
$\rho_0^{\&}$ (Ω -cm)	7	7
n_0 or p_0 (cm^{-3})	5.95×10^{14}	1.98×10^{15}
μ_{e0} or μ_{h0} ($\text{cm}^2/\text{V-s}$)	1,500	500
ρ (Ω -cm)	2.2×10^5	1.6×10^5
n or p (cm^{-3})	2.0×10^{11}	4.8×10^{11}
μ_e or μ_h ($\text{cm}^2/\text{V-s}$)	137	81

Table 1. Hall measurement* results of proton bombarded n & p type Si wafers^v

	Case 1	Case 2
Sample	n-Si, 7 Ω -cm	n-Si, 7 Ω -cm
n_0 (cm^{-3})	$5.95 \cdot 10^{14}$	$5.95 \cdot 10^{14}$
Proton fluence F (cm^{-2})	$7.16 \cdot 10^{15}$	$3.58 \cdot 10^{16}$
N_T (cm^{-3}) ^v	$2.29 \cdot 10^{18}$	$1.15 \cdot 10^{19}$
n (cm^{-3}) [#]	$2.75 \cdot 10^{10}$	$4.38 \cdot 10^9$
E_F (eV)	0.0415126	-0.0044588
E_T (eV)	0.2478826	0.2421732
δ (eV)	$1.2 \cdot 10^{-6}$	$2.0 \cdot 10^{-7}$

final n is still larger than p

Table 2. Extracted parameters of proton-treated n-Si, based on single-level mode

	Case 1	Case 2
Sample	p-Si, 7 Ω -cm	p-Si, 1,000 Ω -cm
p_0 (cm ⁻³)	1.98 · 10 ¹⁵	1.389 · 10 ¹³
Proton fluence F (cm ⁻²)	2.30 · 10 ¹⁶	1.56 · 10 ¹⁵
N_T (cm ⁻³) [♥]	7.36 · 10 ¹⁸	3.48 · 10 ¹⁸
p (cm ⁻³) [#]	4.72 · 10 ¹¹	7.04 · 10 ⁹
E_F (eV)	-0.1372976	-0.03216341
E_T (eV)	-0.3428148	-0.3429603
δ (eV)	6.0 · 10 ⁻⁷	1.27 · 10 ⁻⁵

final p is still larger than n

Table 3. Extracted parameters of proton-treated p-Si, based on single-level model[∇]

Superscripts for Tables 2 and 3

[∇] all energy levels are measured from center of energy band-gap, so $E_C = 0.56$ eV, $E_V = -0.56$ eV; at 300 K, $N_C = 2.8 \cdot 10^{19}$ cm⁻³, $N_V = 1.04 \cdot 10^{19}$ cm⁻³.

[♥] Total defect number density N_T was obtained from TRIM simulation

Standing-laser-poling for Implementing Short-Pitch Periodic Domain Inversion In Ferroelectric Media

Chungpin Liao, Chien-Jung Liao, Tsun-Neng Yang, and Shan-Ming Lan

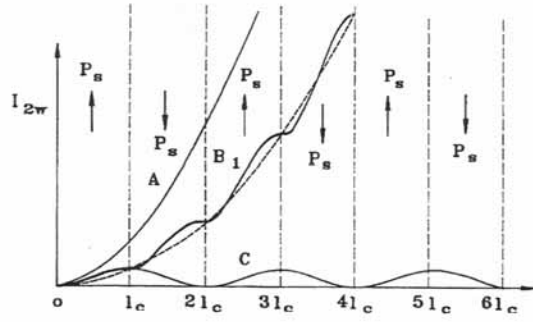
Abstract -- A special “standing-laser-poling” method for volumetric domain inversion of nonlinear ferroelectric media, such as LiNbO_3 , is proposed. Using the combination of a short-wavelength high-field laser standing wave pattern and a background electric field, a short-period bulk domain inversion pattern may be naturally and sharply formed within the nonlinear media.

Index-terms – Electro-poling, Lithium niobate, Second harmonic generation, Standing laser wave

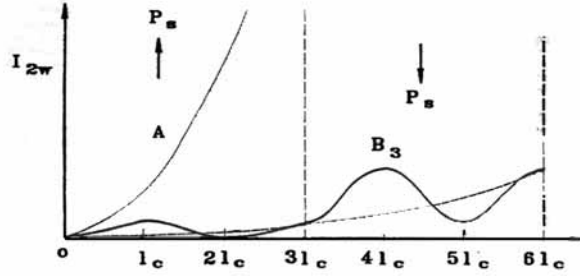
I. INTRODUCTION

Nonlinear optics is concerned with the optical properties of matter in intense radiation fields, such as those produced by a laser or a coherent source of EM wave. The optical nonlinearity of a material results from an anharmonic (and usually anisotropic as well) restoring force when an electron is perturbed by an electric field (or electromagnetic field). For example, in lithium niobate (LiNbO_3), the restoring force is stronger for perturbations along the direction of the inbuilt electric field than for perturbations opposed to the inbuilt field. Unlike the situation in linear optical materials at low light intensities, the electromagnetic polarization induced by nonlinear optical materials responds nonlinearly to the electric field of the light. This in turn can give rise to a variety of optical phenomena that can be used to manipulate light, e.g., optical harmonic generation, Raman scattering, parametric amplification, and intensity-dependent refractive indices.

Ferroelectric materials, to which lithium niobate belongs, have spontaneous polarization (i.e., inbuilt electric field). That is, these materials have internal electric dipole moments. The direction of these moments can be controlled to form certain desired domain configurations within the ferroelectric media, such as the aforementioned lithium niobate. In this connection, much effort and research have been involved in developing structures having particular domain patterns for optic frequency conversions, in particular the second harmonic generation (SHG). The most favorable approach to this end has been the so-called quasi-phase-matching (QPM) (see Ref. [1] for a comprehensive introduction). It is a technique for phase matching nonlinear optical interactions in which the relative phase between the optic pump wave and the generated second harmonic wave is corrected at regular intervals using a structural periodicity built into the nonlinear media.



(a)



(b)

FIG. 1. shows the effect of phase matching on the growth of second harmonic intensity with distance in a nonlinear crystal.

FIG. 1 shows the effect of phase matching on the growth of second harmonic intensity with distance in a nonlinear crystal. In FIG. 1 (a), curve A corresponds to perfect phase matching at every point along the light wave propagation direction. Curve C represents the situation of non-phase-matched interaction. Curve B_1 gives the desired first-order QPM by flipping the sign of the spontaneous polarization (P_s) every coherent length (l_c) of the interaction curve C. Note that when l_c is very small, curve B_1 is approaching the ideal curve A. Additionally, in FIG. 1 (b), with curve A still representing perfect phase matching, curve B_3 reflects the less favorable situation of third-order QPM by flipping P_s every three coherent lengths.

Much of the interest in second harmonic generation (SHG) is due to the increasing possibility that frequency conversion via domain periodic patterning will provide reliable, inexpensive, and compact sources of desired radiation having adequate color (or, frequency) for its purposes. In particular, much of the current attention is devoted to generating blue optical radiation, of wavelength in the range of about 400-450 nm from a near-IR pump laser, for the realization of next generation (15 GB) DVD (digital video disc) data read/write heads as well as the blue laser light source for the projection TVs. However, these applications require short-pitch (i.e., short domain inversion period, about 1.67 μm at room temperature for the congruent lithium niobate frequency converters [2][3].

Existing domain patterning methods can roughly be divided into two categories, namely, the shallow modulation and the deep (volumetric) domain inversion. The former can be accomplished by various ways. They are, e.g., location-selective electron beam scanning (see, e.g., [4]), ion beam scanning (see, e.g., [5]), focused laser beam scanning (see, e.g., [6]), proton exchange of various versions on the nonlinear crystal surface (see, e.g., [7], [8]). Although these shallow approaches can render favorable short-period (2-4 microns) domain patterning, the resultant active QPM regions are usually of less than 2 microns depth. This makes aligning the active regions with a single-mode optic fiber of normal core diameter of 8-10 microns very hard, and usually necessitates the construction of a waveguide.

What's more, due to the resultant non-perpendicular domain walls, the efficiency of such second harmonic generation is always lower than that of the case with a volumetric domain inversion. Our proposed method is in the more favorable category of volumetric domain inversion.

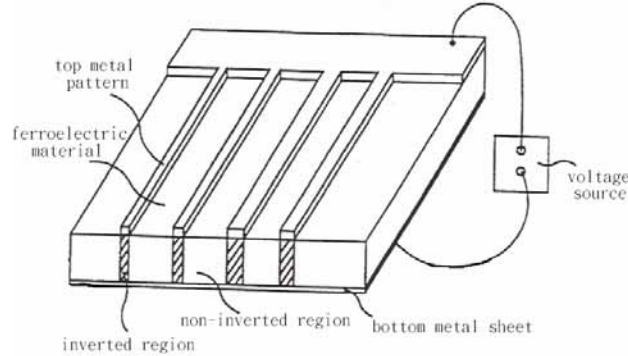


FIG. 2. illustrates the setup of existing electro-poling method to volumetrically pattern the nonlinear crystal.

II. EXISTING METHODS FOR VOLUMETRIC DOMAIN INVERSION

One popular approach to the volumetric domain patterning of a ferroelectric material for quasi-phase-matching (QPM) is by applying an electric field to that material to change the direction of spontaneous polarization at desired locations. This is commonly referred to as the electric field poling or electro-poling (see FIG. 2, wherein a top metal pattern and a bottom metal sheet on the ferroelectric material are biased by the voltage source, leading to domain inverted regions and non-inverted regions). There is a long list of existing practices related to variations of this method (e.g., [9], [10]). In this connection, ferroelectric materials to be electro-poled are often prepared in bulk form having spontaneous polarization in a single direction. To achieve efficient quasi-phase-matching, namely the first order QPM-SHG (see FIG. 1), adjacent domains are made to be of reversed directions of polarization. This has been routinely accomplished by the large, pulsed electric field in the range of 20-26 kV/mm (e.g., for LiNbO₃), with the width of each domain being about equal to one “coherent length” or period l_c , of the desired nonlinear wave interaction within. Here the coherent length means the distance over which the phases of the original optical radiation and the generated double-frequency optic radiation slip by 180 degrees. That is,

$$\Delta k \cdot l_c = \pi \quad (1)$$

where Δk is the difference of wave numbers ($k = 2\pi/\lambda$, λ is wavelength) between the pump laser and its radiated second harmonic wave within the patterned nonlinear media, and is often called the “mismatch.” With access to smaller period l_c , more mismatch is allowed in generating second harmonic light. Hence, it is highly desirable to have short inversion period l_c in order to have wide QPM-SHG operating window and high frequency conversion efficiency [1].

Two major problems associated with the traditional electric field poling are that it is difficult to provide short period (i.e., small l_c) domain inversion patterning and high-resolution domain wall between adjacent domains. The reasons are found to be electric field diffusion in the ferroelectric materials and the hardly avoidable fringe field (see, e.g., [11]). That is, when a large electric field is applied between two contact electrodes (say, in the vertical direction, see, FIG. 2), across a ferroelectric crystal (say, placed horizontally), the electric field distribution tends to broaden (or diffuse) horizontally within the crystal. This practically limits the formation of volumetric domain inversion to a minimum period of about 6 microns on a piece of, e.g., LiNbO₃ crystal of about 500 microns thickness. As indicated by

equation (1), this large period means hard QPM-SHG frequency conversion. In particular, other sources of mismatch arising from fabrication error or changes of fundamental wavelength and temperature, etc. can lead to more detuning effects which further reduce the QPM bandwidth and the SHG conversion efficiency (see, e.g., [1], [12]).

It is for this reason, a doping scheme was proposed [13] to increase the resistivity of the crystals in an attempt to suppress the electric field diffusion difficulty. However, all existing efforts have not brought satisfactory results. In fact, this is why, up to the present day, we hardly see less-than-6-micron-pitch bulk SHG crystals.

From the application point of view, this poses a severe limit to a lot of frequency converting schemes. For example, 1st-order SHG blue light practically cannot be generated from a bulk lithium niobate of large inversion pitch, and thus people are only left with the less favorable 3rd-order options.

III. THE PROPOSED METHOD

Our proposed method utilizes short-wavelength (e.g., 0.2-2 microns), pulsed high-field laser standing wave pattern to realize short-period volumetric domain inversion in the nonlinear media, such as lithium niobate (LiNbO₃). It is this short laser wavelength that will automatically force the domain inversion period within the nonlinear media to be about half the laser wavelength. Note, however, that although the nodes of a standing wave do not change their positions in either time or space, the standing wave amplitude and direction between them do change in time as $\cos(\omega t)$, where $\omega(=2\pi f)$, f is frequency) is the high-field laser angular frequency. Thus, in order to periodically establish domain inversion within the nonlinear media (e.g., LiNbO₃) using standing laser wave pattern, an extra background field E_{back} is needed. For example, a uniform DC electric field can be applied. That is, suppose the threshold electric field to cause domain inversion in that nonlinear media is E_{th} , then to realize the invented method, it is necessary to make both E_{back} and the peak standing wave amplitude E_0 less than E_{th} , respectively; while requiring E_{back} plus E_0 (i.e., when the two point in the same direction) to be greater than or equal to E_{th} .

For the existing electro-poling methods, a mask-patterned electric field of about 20-26 kV/mm is applied on LiNbO₃ for about 50 μs to several seconds each time. (The required electric field strength has been known to be lower if the treated nonlinear crystal was properly heated.) For the proposed standing-laser-poling method, if the chosen laser wavelength is about 1 μm , then existing high-power (1-10 MW) pulsed lasers such as YAG can be employed. Since the laser frequency is in the 10^{14} Hz range, the suggested standing-laser-poling is in fact achieved by repeated poling actions within the applied, say, 10 ms laser pulse duration.

In order to create domain inversion of a desired period l_c within the nonlinear media, a standing wave electric field pattern of period l_c is needed. This would require a high-field laser of wavelength $\lambda \approx 2 \cdot l_c$ together with a background (e.g., constant uniform DC) electric field as illustrated in FIGs. 3 and 4. The background field is realized, for example, by two biased parallel metal plates. An example of the setup is as follows. If an inversion period of $l_c \approx 0.5 \mu\text{m}$ is desired, then a high-field laser of wavelength $\lambda \approx 1 \mu\text{m}$ is employed to form a laser standing wave pattern, by using a beam splitter and mirrors. The desired poling standing wave pattern, of period of about 0.5 μm , emerges from the combination of standing wave and background field. Though oscillating temporally in amplitude, the poling standing field pattern pulls the nonlinear media to render domain inversion in a patterned fashion every time when reaching its peak field in the same direction of the DC field.

Namely, to realize the proposed method, it is necessary to have both the background DC field E_{dc} and the peak

standing wave amplitude E_0 less than the threshold field E_{th} for domain inversion, respectively, while requiring their sum to be greater than or equal to E_{th} . Take LiNbO_3 for an example. If the required threshold electric field to cause domain inversion within LiNbO_3 is 26 kV/mm along a chosen crystal axis and facet, then it can be arranged, for example, such that $E_{dc} \approx 14$ kV/mm, and the peak laser electric field $E_0 \approx 14$ kV/mm, say. There are simply many workable combinations of E_{dc} and E_0 values to carry out the proposed method.

The required laser pulse power can be calculated as follows. The corresponding peak laser power is about $E_0 H_0 A$, where the magnetic field intensity H is equal to B/μ_0 , in which $\mu_0 (= 4\pi \cdot 10^{-7}$ Henry/m) is the magnetic permeability, B is the magnetic flux density, and A is the laser beam cross-sectional area. Assuming TEM wave for the high field laser beam (see the setup in FIG. 3), such that B is equal to E_0/c ($c = 3 \cdot 10^8$ m/s), and for a beam diameter of $D \approx 1$ cm, then the desired laser power is about 35 MW. There are quite a few existing choices for pulsed lasers of this power level and of wavelengths in the 0.2-4 μm range. For example, according to [14], at least several high-power pulse-type lasers are available:

Table1 : high-power pulse-type lasers

Type	Wavelength (μm)	Pulsed power level (W)
Holmium	2.06	$>10^7$
Iodine	1.315	$>10^{12}$
Nd-glass, YAG	1.06	$\sim 10^{14}$
Ruby	0.6943	10^{10}
Kr-F	0.26	$>10^9$
Xenon	0.175	$>10^8$

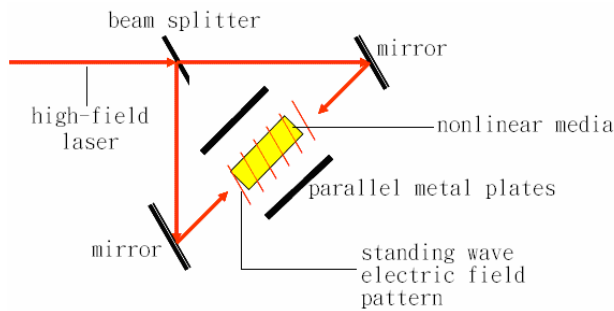


FIG. 3. shows the setup of the proposed standing-wave laser-poling method.

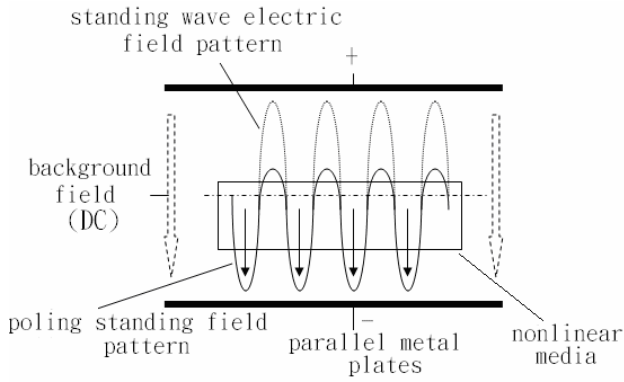


FIG. 4. illustrates the detailed combined action of the proposed standing laser field and the background field.

IV. SUMMARY AND CONCLUSIONS

A novel method [15] is proposed to implement short-pitch periodic domain inversion on ferroelectric media, which utilizes short-wavelength (e.g., 0.2-2 microns), pulsed high field laser standing wave pattern to realize short-period volumetric domain inversion in the nonlinear media, such as lithium niobate (LiNbO_3). It is this short laser wavelength that will automatically force the domain inversion period within the nonlinear media to be about half the laser wavelength. Note, however, that although the nodes of a standing wave do not change their positions in either time or space, the standing wave amplitude and direction between them do change in time as $\cos(\omega t)$, where $\omega (= 2\pi f)$, f is frequency) is the high-field laser angular frequency. Thus, in order to periodically establish domain inversion within the nonlinear media (e.g., LiNbO_3) using standing laser wave pattern, an extra background field E_{back} is needed. That is, to realize the invented method, it is necessary to make both E_{back} and the peak standing wave amplitude E_0 less than the threshold electric field E_{th} , respectively; while requiring E_{back} plus E_0 (i.e., when the two point in the same direction) to be greater than or equal to E_{th} . Further, it is estimated that existing high-power (~ 10 MW) pulsed lasers of desired wavelengths can be employed. Since the laser frequency is in the 10^{14} Hz range, the suggested standing-laser-poling is in fact achieved by repeated poling actions within the applied, say, 10 ms laser pulse duration.

When short-pitch periodic poling can be achieved, another very important category of applications is the manufacturing of so-called photonic crystals. Just as a process-patterned silicon crystal would direct electron flows in a desirable way, a properly patterned photonic crystal would do the same to light. By changing the size, distribution and periodicity of its ferroelectric domains, the properties of a PPLN (periodically poled lithium niobate) crystal, now known as a “designer” material, can be engineered to match the requirement of a given light-manipulation application.

ACKNOWLEDGMENT

The authors would like to express their gratitude to ARBL, INER and NSC (National Science Council) for their technical supports to this research.

- [1] Fejer, M. M., “Quasi-Phase-Matched Second Harmonic Generation: Tuning and Tolerances,” *IEEE Journal of Quantum Electronics*, Vol. 28, No. 11, 1992.
- [2] Nelson, D. F. and Mikulyak, *J. Appl. Phys* **45**, 3688 (1974).
- [3] Jundt, D. H., *Optics Letters*, **22**, 1553 (1997).
- [4] Fujimura, M. et al., “Blue light generation in LiNbO_3 waveguide SHG device with first order domain-inverted grating formed by EB

scanning," *Electronics Letters*, Vol. 28, No. 20, 1992.

- [5] Mizuuchi, K. and Yamamoto, K., "Domain inversion in LiTaO₃ using an ion beam," *Electronics Letters*, Vol. 29, No. 23, 1993.
- [6] Daneshvar, K. and Kang, D. H., "A novel method for laser-induced periodic domain reversal in LiNbO₃," *IEEE J. Quantum Electronics*, Vol. 36, No. 1, 2000.
- [7] Bortz, M. L. et al., "Noncritical quasi-phase-matched second harmonic generation in an annealed proton-exchanged LiNbO₃ waveguide," *IEEE Trans. Quantum Electronics*, Vol. 30, No. 12, 1994.
- [8] Kawaguchi, T., Yoshino, T., Imaeda, M., Mizuuchi, K., Yamamoto, K., "Optical waveguide element, optical element, method for producing optical waveguide element and method for producing periodic domain-inverted structure," US Patent 5,943,465, August 24, 1999.
- [9] Byer, R. L., Fejer, M. M., Lim, E. J., "Method of controlling regions of ferroelectric polarization domains in solid state bodies," US Patent 5,714,198, Feb. 3, 1998
- [10] Field, S. J. and Deacon, D. A. G., "Fabrication of patterned poled dielectric structures and devices," US Patent 5,615,041, March 25, 1997
- [11] Kintaka, K., Fujimura, M., and Nishihara, H., "High-efficiency LiNbO₃ waveguide second-harmonic generation devices with ferroelectric-domain-inverted gratings fabricated by applying voltage," *J. Lightwave Technology*, Vol. 14, No. 3, 1996.
- [12] Wu, J., Kondo, T., and Ito, R., "Optimal design for broadband quasi-phase-matched second-harmonic generation using simulated annealing," *J. Lightwave Technology*, Vol. 13, No. 3, 1995.
- [13] Karlsson, H., Arvidsson, G., Henriksson, P., Laurell, F., "Method and arrangement for poling of optical crystals," US Patent 5,986,798, Nov. 16, 1999
- [14] US Naval Research Laboratory, *Plasma Formulary*, p. 50, 1987.
- [15] Several key patents are being applied by both NFU and ARBL.

Dr. Chungpin Liao was born in 1959 at Taichung, Taiwan, R.O.C. He received his B.S. degree in Nuclear Engineering from National Tsing-Hua University, Hsinchu, Taiwan, R.O.C., in 1982; and M.S. and Ph.D. degrees in Plasma Science and Fusion Technology from MIT at Cambridge, MA, USA in 1989 and 1992, respectively. After 4 years of research fellow at MIT, he returned to Taiwan in May 1995 to join ERSO (Electronic Research and Services Organization) of ITRI (Industrial Technology Research Institute), and eventually left ITRI at the end of July 2000 to become the founding CEO of ARBL (Advanced Research & Business Laboratory), an adventure focused on the integration and innovation of multi-disciplinary fields including nanotechnology, photonics, chemistry, electromagnetism, electronics, medical science, and quantum computing. Beginning September 2003, Dr. Liao also serves as Associate Professor of the Graduate School of Electro-Optic and Material Science of the National Formosa University (NFU), Taiwan. Now, while making himself busy with mandated research services from different fields, he is further devoting much of his energy in materializing his cross-disciplinary ideas by inventing new products and technologies, for example, frequency doubler for blue light generation, Kirlian photography, and even psychokinetic coherent controls, etc.

Mr. Chien-Jung Liao was a special topic student 2004 -2005 of Prof. Chungpin Liao. He is now in the Graduate School of Opto-electronics of the National Tsing-Hua University.

Dr. Tsun-Neng Yang was born in 1951 in Taiwan. He obtained his Ph.D. from National Tsing Hua University, and currently is an active Researcher in the Physics Division of INER (Institute of Nuclear Energy Research). His main research effort now is focused on areas including the proton implantation in VCSEL, RCLED, etc., optic communication devices, and silicon quantum dots in LED and solar cell applications.

Dr. Shan-Ming Lan currently works for the Nuclear Instruments Division of INER. His major focus of research has been the semiconductor and optoelectronic material properties.

To be further modified and submitted to an international journal

Creation of Resonance Frequencies and Enhancement of K by Collective Defect Interactions and Their Novel Applications

Chungpin Liao^{1,2}, Hsien-Ming Chang¹, Tsun-Neng Yang³, Shan-Ming Lan³

¹Graduate School of Electro-Optical and Material Science,

National Formosa University (NFU), Huwei, Taiwan, ROC

²Advanced Research & Business Laboratory (ARBL), Taichung, Taiwan, ROC

³Institute of Nuclear Energy Research (INER), Lungtan, ROC

cpliao@alum.mit.edu

Tel: +886-936-767-719

Abstract—In optical and photonic applications, it will be most desirable to have available some resonance frequencies (Ω 's) in the index of refraction (n) of a specific material or device, such that the desired spectral properties can be secured, e.g., to create some resonance peak, or resonance absorption spectrum around certain frequency; Or, to alter the shape of the refractive index vs. frequency curve. However, in natural or man-made bulk materials, such resonance frequencies are fixed, and therefore are not necessarily at frequencies of desire. One existing common approach is via implementing quantum dots or making quantum well structures on the host material, and allowing the quantum mechanics to take effect. However, such “quantum mechanical” effort always put stringent requirements on the intricacy of all related processing tools and materials. Here, instead, we'll look for more “classical” alternatives, such as the collective defect engineering approach. In this defect dipole approach, extra dipoles of desired resonance frequencies, in the form of molecules, crystal defects, nano-structures, are incorporated into the host materials to alter its optical properties. In the cases where the desired dipoles of favorable resonance frequencies are not available, or even hard to synthesize, we'll demonstrate, via the Clausius-Mossotti equation (CME), that the collective co-working of more than one type of implemented defect dipoles may be utilized to generate the resonance at the desired frequency. In other words, the now created resonance is as if caused by some “phantom” resonating defects at the desired frequency. (Here, it is emphasized that the CME is used to describe the added extra defect dipoles, not the host bulk material traditionally.) An example of “forward-shifted” resonance will be given. Further, a novel idea of “strange mirror” will be presented in which a light impinging on it at certain incident angle is bounced at a very different reflection angle. The latter may find its use in many areas, for example, the light coupling into an optic fiber.

Keywords—Generation of desired resonance frequency, Collective dipole interaction, Clausius-Mossotti equation, Dispersion relation, Defect engineering, Dipole engineering

INTRODUCTION

In various application domains of optics and electro-optics,

it is often favorable to have available within materials or devices resonance peaks in the refraction index (or resonance absorption) at the desired frequencies. When they are naturally unavailable, people usually turn to the option of implanting artificial dipole moments, in the form of specific molecules or compounds, which manifest resonance at such frequencies. But if even such add-ins are nonexistent or cannot be easily synthesized, there are some other high-tech options left. One popular approach is embedding quantum dots in a host material, or equipping the latter with the quantum well structure of a suitable topology. However, such “quantum mechanical” effort always put stringent requirements on the intricacy of all related processing tools and materials. Here, instead, we'll look for more “classical” alternatives, such as the collective defect dipole engineering approach. Namely, predetermined extra dipoles will be incorporated in an original “host material” in a way to considerably alter the optical and electro-optical properties of the latter.

The dispersion relation describes the spectral property of a substance, i.e. a relation between ω and k , which ultimately determines the characteristics of the substance's relative dielectric coefficient ϵ_r . In the above, ω is the radian frequency of light propagating within the substance and $k = 2\pi/\lambda$ is the wave number of the light. For solid, nonmagnetic optical and electro-optical materials, the somewhat appropriate dispersion relation has conventionally been the so-called Clausius-Mossotti equation [1][2], which stemmed from treating atoms (including nuclei and electrons) as light-reacting electric dipoles. It is emphasized, however, in contrast to the traditional use of the Clausius-Mossotti equation (hereafter, CME) for a specific material, here instead

the CME is only employed to describe the reactive response to light of varying frequencies of those extra dipoles incorporated within a host material.

It was realized through investigating the CME that by incorporating two or more types of electric dipoles in a host material, the resultant collective resonance can in principle be materialized at any targeted frequency we desire where there existed no resonance originally. Namely, one or more “phantom” resonance(s) can be created without the existence of corresponding physical resonators. This, in fact, is due to the collective coupling among the two or more types of dipole moments we put in the host material. Since the such-generated phantom frequencies are normally different from those natural ones associated with each participating added dipoles the phenomenon might also be termed the “resonance shifting.” In the following, we will take the “forward-push” of the collective resonance as an example to show the detailed adjustment of physical parameters in CME required to significantly bring forth the phenomenon. We anticipate that this “resonance shifting” effect will help cultivate many more important engineering applications [3].

CLAUSIUS-MOSSOTTI EQUATION (CME) AND A FIRST-ENCOUNTERED “FORWARD-PUSH” OF RESONANCE

The well-known Clausius-Mossotti equation (CME) [1][2] takes the form:

$$(\varepsilon_r - 1)/(\varepsilon_r + 2) = Ne^2 / (3\varepsilon_0 m_e) \cdot \sum_j f_j / (\Omega_j^2 - \omega^2 + i\gamma_j \omega). \quad (1)$$

where N is the total number density of electric dipoles incorporated in the host material, ε_r ($\equiv K$) is the relative permittivity representing the whole cluster of added dipoles, e is the electric charge of an electron, ε_0 is the permittivity of free space, m_e is the rest mass of a electron, f_j is the ratio of the j^{th} type dipoles in the total number density N of added dipoles, Ω_j is the natural radian frequency of the j^{th} type dipoles, γ_j stands for the phenomenological damping radian frequency of electrons [1][2], a is the radian frequency of light propagated in the material, and $i = \sqrt{-1}$.

During the initial phase of our numerical experiments, it was occasionally noticed that when two or more types of electric dipoles were mixed together, a peculiar phenomenon sometimes arose in which the resultant collective resonance frequency was found smaller (or greater) than the natural resonance frequencies of all participating dipoles.

Figure 1 shows the result of mixing two types of electric dipoles. The first type dipoles were of the resonance frequency 7.29×10^{12} Hz (see Fig. 1 (a)) and the added number density

was $2 \times 10^{23} \text{ m}^{-3}$. The second type dipoles were of the resonance frequency 1.59×10^{13} Hz and the added number density was $1.2 \times 10^{25} \text{ m}^{-3}$. We found that the collective resonance frequency was 6.69×10^{12} Hz (see Fig. 1(b)), lower than the natural frequency of the first type dipoles. Thus, a new resonance frequency emerged and was at a “forward-shifted” frequency position. In the following, we’ll attempt to disentangle the CME ingredients and seek the analytic cause of the above effect.

MATHEMATICAL ANALYSIS

Noting that the polarizability of the j^{th} type of dipoles is $e^2 / (\varepsilon_0 m_e \Omega_j^2) = \alpha_j$ and further letting $\gamma_j = 2\gamma_j'$ to comply with the convention, the CME can be normalized into the form:

$$\frac{\varepsilon_r - 1}{\varepsilon_r + 2} = \sum_j \frac{\frac{1}{3} N_j \alpha_j}{1 - x_j^2 + i2x_j y_j} \quad (2)$$

Then, by defining $N_j \equiv N \cdot f_j$, $x_j = a / \Omega_j$, and $y_j = \gamma_j' / \Omega_j$, Eq. (2) is further rewritten as:

$$(\varepsilon_r - 1)/(\varepsilon_r + 2) = \sum_j (1/3) N_j \alpha_j / (1 - x_j^2 + i2x_j y_j). \quad (3)$$

When there exists only one type of dipoles, Eq. (3) is reduced to (using $\varepsilon_r - 1 \equiv z$, and $\frac{1}{3} N_1 \alpha_1 \equiv a_1$):

$$\frac{z}{z+3} = \frac{a_1}{1 - x_1^2 + i2x_1 y_1}, \quad \text{and thus,}$$

$$z \equiv \varepsilon_r - 1 = \frac{3a_1}{(1 - a_1 - x_1^2) + i2x_1 y_1}. \quad \text{Therefore, the resonance occurs at } x_1^2 \cong (1 - a_1), \text{ or } \omega_{res}^2 \cong (1 - a_1)\Omega_1^2.$$

For the sake of mathematical simplicity in addressing the collective mixing of dipoles, we consider here only the situation in which only two types of dipoles are involved. The corresponding CME is (defining $\varepsilon_r - 1 \equiv z$, and $\frac{1}{3} N_j \alpha_j \equiv a_j$):

$$\frac{z}{z+3} = \frac{a_1}{1 - x_1^2 + i2x_1 y_1} + \frac{a_2}{1 - x_2^2 + i2x_2 y_2}$$

$$= \frac{a_1(1 - x_2^2 + i2x_2 y_2) + a_2(1 - x_1^2 + i2x_1 y_1)}{(1 - x_1^2 + i2x_1 y_1)(1 - x_2^2 + i2x_2 y_2)} \quad (4)$$

In the case of low damping of interest we could find that as $y_1 \cong y_2 \cong 0$, ε_r is significant and Eq. (4) becomes:

$$(1-x_1^2)(1-x_2^2)z \equiv [a_1(1-x_2^2) + a_2(1-x_1^2)]z + 3[a_1(1-x_2^2) + a_2(1-x_1^2)] \quad (5)$$

Or,

$$[(1-a_1-a_2)-(1-a_2)x_1^2-(1-a_1)x_2^2+x_1^2x_2^2]z \approx 3[a_1(1-x_2^2)+a_2(1-x_1^2)] \quad (6)$$

Therefore,

$$[(1-a_1-a_2)\Omega_1^2\Omega_2^2-(1-a_2)\Omega_2^2\omega^2-(1-a_1)\Omega_1^2\omega^2+\omega^4]z \approx 3a_1\Omega_1^2(\Omega_2^2-\omega^2)+3a_2\Omega_2^2(\Omega_1^2-\omega^2) \quad (7)$$

From this equation we know that the peak value of z or ϵ_r occurs where the left hand side of Eq. (7) approaches zero.

By letting $[(1-a_2)\Omega_2^2+(1-a_1)\Omega_1^2]=M$, the solution of Eq. (7) is obtained:

$$\omega_{res}^2 = \frac{M \pm \sqrt{M^2 - 4(1-a_1-a_2)\Omega_1^2\Omega_2^2}}{2} = \frac{M \pm M \left(1 - \frac{4(1-a_1-a_2)\Omega_1^2\Omega_2^2}{M^2}\right)^{0.5}}{2} \quad (8)$$

If $\Omega_2^2 \gg \Omega_1^2$, further expansion and omission of higher order terms would lead to:

$$\omega_{res}^2 = \frac{M \pm M \left(1 - \frac{2(1-a_1-a_2)\Omega_1^2\Omega_2^2}{M^2}\right)}{2} \quad (9)$$

Thus, ω_{res}^2 may approximately adopt the following two values (one for “+”, and the other for “-”):

$$(a) \quad \omega_{res}^2 \equiv (1-a_2)\Omega_2^2 + (1-a_1)\Omega_1^2, \text{ and}$$

$$(b) \quad \omega_{res}^2 \equiv (1-a_1-a_2)\Omega_1^2\Omega_2^2 / [(1-a_2)\Omega_2^2 + (1-a_1)\Omega_1^2].$$

In (a), we obtain $a_{res} > \max(\Omega_1, \Omega_2)$ when with both a_1, a_2 very small. On the other hand, in (b), when $\Omega_2^2 \gg \Omega_1^2$, we obtain:

$$\omega_{res}^2 \equiv \frac{1-a_1-a_2}{1-a_2}\Omega_1^2 \quad (10)$$

If a_{res} in Eq. (10) is smaller than that derived for the case involving only a single dipole type (i.e., $\omega_{res}^2 \equiv (1-a_1)\Omega_1^2$), then a collective “forward-shifted” resonance can be achieved. Indeed, since $1-a_2 > 0$, and $(1-a_1-a_2) < (1-a_1)(1-a_2)$, such existence of the “forward-shifted” resonance is evidenced analytically, and its cause (mainly, $y_1 \equiv y_2 \equiv 0, a_1 \ll 1$,

$a_2 \ll 1$, and $\Omega_2^2 \gg \Omega_1^2$) is now understood.

A MORE SIGNIFICANT NUMERICAL RESULT

Figure 2 shows the result of embedding two types of dipoles in a host material, in which $N_1 = 1 \times 10^{23} \text{ m}^{-3}$, $\Omega_1/2\pi = 1 \times 10^{13} \text{ Hz}$ (and $y_1 = 5 \times 10^{-4}$, $a_1 = 0.0269$) and $N_2 = 3 \times 10^{25} \text{ m}^{-3}$, $\Omega_2/2\pi = 3 \times 10^{13} \text{ Hz}$ (and $y_2 = 5 \times 10^{-4}$, $a_2 = 0.8960$). Namely, the created resonance peak is at $6.9 \times 10^{12} \text{ Hz}$, lower than the natural resonance frequencies of both types of participating dipoles.

POSSIBLE APPLICATIONS, INCLUDING A “STRANGE” MIRROR

In principle, once the means of creating resonance within a host material at frequencies of desire is accessible, many reflection types of devices spanning a wide frequency range can be realized. This is because that the refractive index for nonmagnetic materials is $n = (\epsilon_r)^{1/2}$. For example, a material with “phantom dipole”-enhanced refractive index may serve as the wide-band reflector of all incident lights [3].

Further, a “strange” mirror manifesting unequal incident and reflected angles for a monochromatic light may be realized. In fact, as illustrated in Fig. 3, a given source of light at a position P above the above “phantom dipole”-caused reflector can have its light reach any point Q also above the mirror by an infinite number of paths, according to the teaching of quantum mechanics. Let’s now chop up and toss out the right hand $\frac{3}{4}$ of the mirror, leaving only the part near points A, B, and C (see Fig. 3). In classical mechanics it is impossible to bounce a ball from point P to point Q using this remaining piece of a lumber, correspondingly, but in the notion of the quantum mechanics we can trick the light into bouncing, say, from point P to A to Q (henceforth L_{PAQ})! Namely, by chopping off regions on the remaining reflector where the light paths (connecting P and Q) are of lengths differing from L_{PAQ} by a non-integer multiples of the light’s wavelength, we then have a series of slats where the light paths bouncing off the slats all have nearly the same phasor orientation. Thus, the constructive interference among these parallel phasors would result in significant ray intensity for the monochromatic light going from point P to point A, and then to point Q. Consequently, a new way of light reflection may be realized which apparently violates the traditional reflection law.

CONCLUSION

In optical and photonic applications, it will be most desirable to have available some resonance frequencies (Ω ’s) in the index of refraction (n) of a specific material or device, such that the desired spectral properties can be secured, e.g., to

create some resonance peak, or resonance absorption spectrum around certain frequency; Or, to alter the shape of the refractive index vs. frequency curve. However, in natural or man-made bulk materials, such resonance frequencies are fixed, and therefore are not necessarily at frequencies of desire. One existing common approach is via implementing quantum dots or making quantum well structures on the host material, and allowing the quantum mechanics to take effect. However, such “quantum mechanical” effort always put stringent requirements on the intricacy of all related processing tools and materials. Here, instead, we looked for more “classical” alternatives, such as the collective defect engineering approach. In this defect dipole approach, extra dipoles of desired resonance frequencies, in the form of molecules, crystal defects, nano-structures, are incorporated into the host materials to alter its optical properties. In the cases where the desired dipoles of favorable resonance frequencies are not available, or even hard to synthesize, we demonstrated, via the Clausius-Mossotti equation (CME), that the collective co-working of more than one type of implemented defect dipoles could be utilized to generate the resonance at the desired frequency. Finally, a novel idea of “strange mirror” was presented in which a light impinging on it at certain incident angle is bounced at a very different reflection angle. The latter may find its use in many areas, for example, the light coupling into an optic fiber.

REFERENCES

- G. Bekefi and A. H. Barrett, *Electromagnetic Vibrations, Waves, And Radiation*, pp. 435-437, MIT Press, Cambridge (1977).
 M. A. Omar, *Elementary Solid State Physics*, pp. 376-384, Addison-Wesley, Reading Massachusetts (1993).
 Patents for advanced applications are being pursued by both NFU and ARBL.

Figure Captions:

Fig. 1. The emergence of a new “forward-shifted” phantom resonance (Fig. 1(b)) as the result of mixing two types of dipoles: $N_1 = 2 \times 10^{23} \text{ m}^{-3}$, $\Omega_1/2\pi = 7.29 \times 10^{12} \text{ Hz}$ (shown in Fig. 1(a)), and $N_2 = 1.2 \times 10^{25} \text{ m}^{-3}$, $\Omega_2/2\pi = 1.59 \times 10^{13} \text{ Hz}$.

Fig. 2. A “forward-push” of resonance frequency of a much larger amplitude, as the result of mixing two types of dipoles: $N_1 = 1 \times 10^{23} \text{ m}^{-3}$, $\Omega_1/2\pi = 1 \times 10^{13} \text{ Hz}$, and $N_2 = 3 \times 10^{25} \text{ m}^{-3}$, $\Omega_2/2\pi = 3 \times 10^{13} \text{ Hz}$.

Fig. 3. An illustration to elaborate the formation of “strange mirror” on a material of collective-dipoles-enhanced refractive index

Figures:

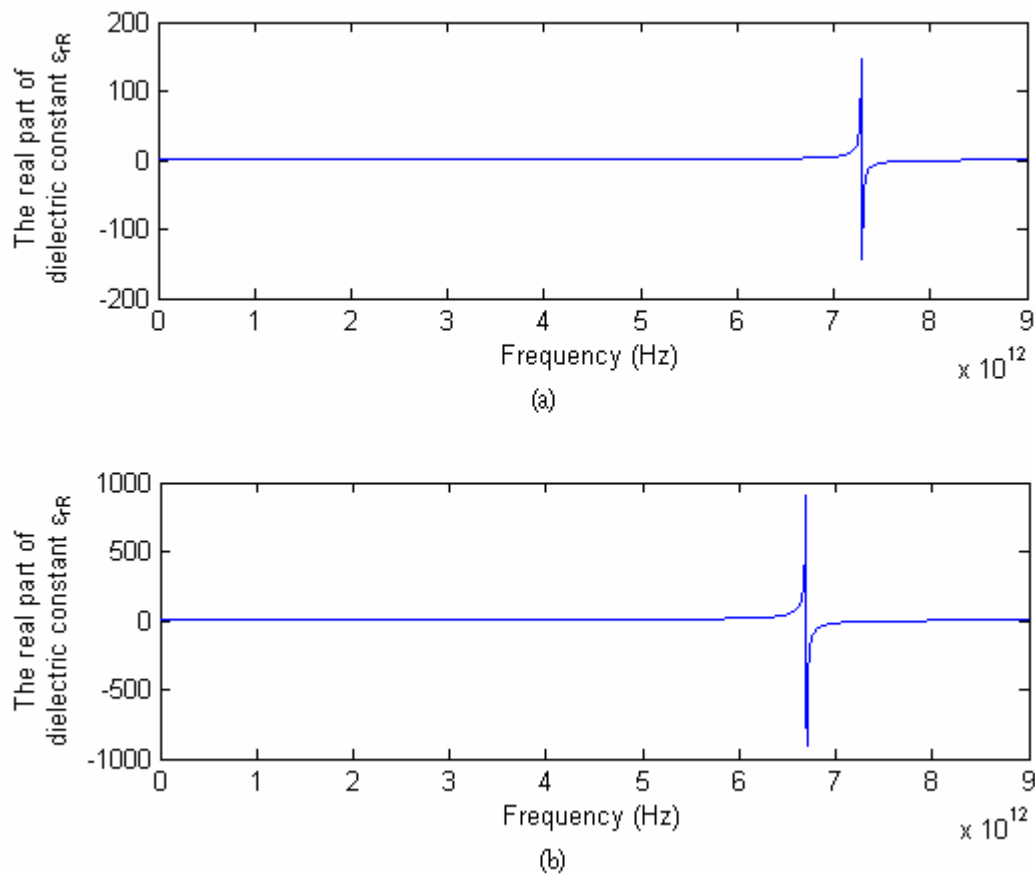


Fig. 1. The emergence of a new “forward-shifted” phantom resonance (Fig. 1(b)), as the result of mixing two types of dipoles: $N_1 = 2 \times 10^{23} \text{ m}^{-3}$, $\Omega_1/2\pi = 7.29 \times 10^{12} \text{ Hz}$ (shown in Fig. 1(a)), and $N_2 = 1.2 \times 10^{25} \text{ m}^{-3}$, $\Omega_2/2\pi = 1.59 \times 10^{13} \text{ Hz}$.

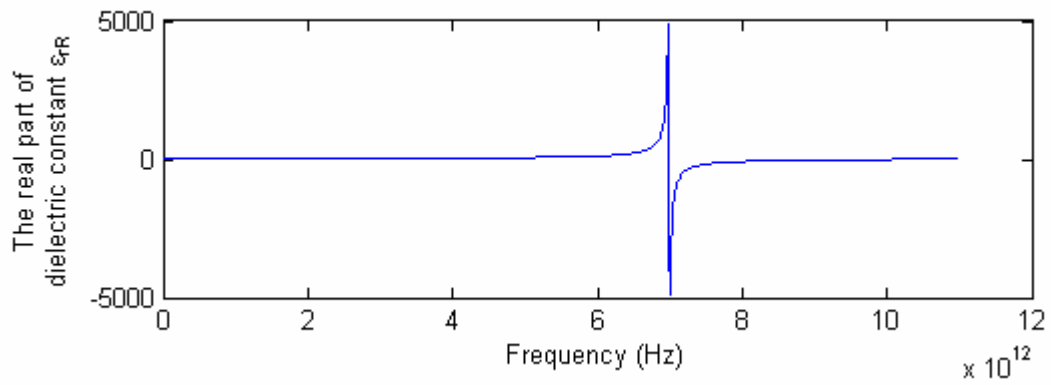


Fig. 2. A “forward-push” of resonance frequency of a much larger amplitude, as the result of mixing two types of dipoles: $N_1 = 1 \times 10^{23} \text{ m}^{-3}$, $\Omega_1/2\pi = 1 \times 10^{13} \text{ Hz}$, and $N_2 = 3 \times 10^{25} \text{ m}^{-3}$, $\Omega_2/2\pi = 3 \times 10^{13} \text{ Hz}$.

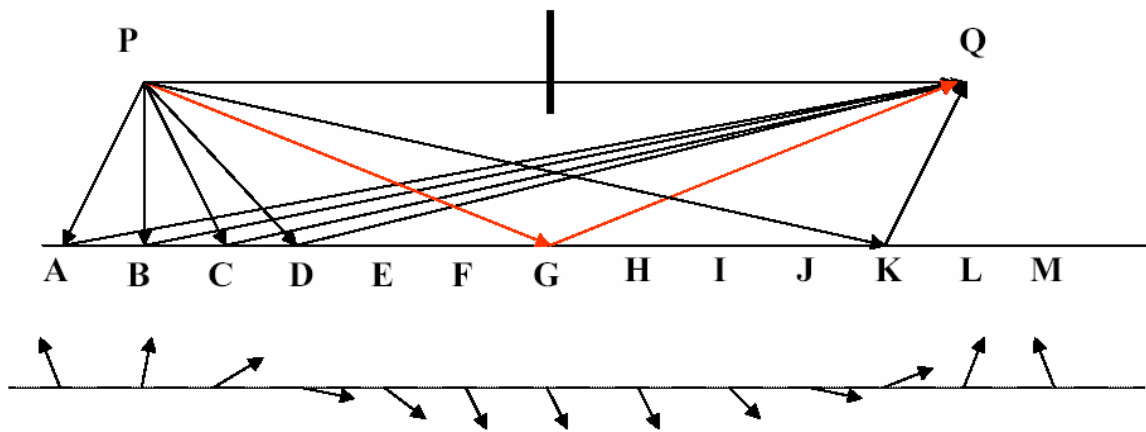


Fig. 3. An illustration to elaborate the formation of “strange mirror” on a material of collective-dipoles-enhanced refractive index